UC Santa Barbara
Recent Work

Title

Periodicity, Chaos and Localization in a Burridge-Knopoff Model of an Earthquake with Dieterich-Ruina Friction

Permalink

https://escholarship.org/uc/item/3r5811tp

Authors

Erickson, Brittany
Birnir, Bjorn
Lavallée, Daniel

Publication Date

2010-08-19

Periodicity, Chaos and Localization in a Burridge-Knopoff Model of an Earthquake with Dieterich-Ruina Friction

Brittany Erickson[1], Björn Birnir[1] and Daniel Lavallée[2]

[1] Department of Mathematics, University of California, Santa Barbara
[2] Earth Research Institute, University of California, Santa Barbara

ABSTRACT

We investigate the emergent dynamics when the nonlinear Dieterich-Ruina rate and state friction law is attached to a Burridge-Knopoff spring-block model. We derive both the discrete equations and the continuum formulation governing the system in this framework. The discrete system (ODEs) exhibits both periodic and chaotic motion, where the system's transition to chaos is size-dependent, i.e. how many blocks are considered. From the discrete model we derive the nonlinear elastic wave equation by taking the continuum limit. This results in a nonlinear partial differential equation (PDE) and we find that both temporal and spatial chaos ensues when the same parameter is increased. This critical parameter value needed for the onset of chaos in the continuous model is much smaller than the value needed in the case of a single block and we discuss the implications this has on dynamic modeling of earthquake rupture with this specific friction law. Most importantly, these results suggest that the friction law is scale-dependent, thus caution should be taken when attaching a friction law derived at laboratory scales to full-scale earthquake rupture models. Furthermore, we find solutions where the initial slip pulse propagates like a traveling wave, or remains localized in space, suggesting the presence of soliton and breather solutions. We discuss the significance of these pulse-like solutions and how they can be understood as a proxy for the propagation of the rupture front across the fault surface during an earthquake. We compute analytically the conditions for soliton solutions and by exploring the resulting parameter space, we introduce a possible method for determining a range of suitable parameter values to be used in future dynamic earthquake modeling.

1 Introduction

1.1 Background

Although significant advances have been made in our knowledge of fault structure and plate tectonics, our understanding of the the physical mechanisms responsible for the initiation, propagation and termination of earthquake rupture remains unclear. It is believed that there exist

1

complex physical properties and behaviors in the earth's crust and along fault surfaces that prevent our ability to make accurate predictions. Two avenues by which we try to understand the physics and complexity of earthquakes are in laboratory studies of rock friction and mathematical dynamic rupture modeling. So far these two fields remain relatively disconnected and it is still unclear how laboratory discoveries can best be applied in dynamic models of earthquake faults [Scholz, 1998], [Marone, 1998].

The late 1970s saw an increased interest in stick-slip instabilities present in laboratory rock experiments as a means of understanding earthquake ruptures. Dieterich, Ruina, Rice and others used these experiments as a means to formulate constitutive laws capable of describing the frictional stress when rocks were sheared against each other or over a surface [Dieterich, 1978], [Ruina, 1983], [Rice, 1983]. The mechanisms of slip instabilities in laboratory experiments have been proposed to be dependent on several factors including reduced frictional force during sliding (slip weakening) and a decrease in slip velocity [Ruina, 1983]. Improvements to these constitutive laws were made when data analysis suggested that friction could not be a function solely dependent on velocity, nor could slip-weakening friction completely describe the relationship between static and dynamic friction [Marone, 1998].

Resolution to these setbacks were made when they found that with the incorporation of a state variable there emerged a robust friction law capable of reproducing a wide range of dynamics similar to the behavior of a fault during an earthquake rupture. These emergent dynamics include a Gutenberg-Richter distribution of event sizes, stick-slip phenomena and fault healing [Marone, 1998]. The state variable is an empirical quantity usually interpreted as a measure of asperity contact between two sheared surfaces, or the amount of time required for the renewal of these asperities (characteristic contact lifetime) [Marone, 1998].

1.2   The "Slip Law" Formulation

In the literature this constitutive law is currently referred to as "rate and state" friction or the "Dieterich-Ruina" (D-R) friction law. One formulation of such a friction law was proposed by Ruina [1983] and is known as the "slip law" [Ampuero and Rubin, 2007]:

$$\left.\begin{array}{l} \tau = \sigma[\mu_o + \theta + A\ln(\frac{V}{V_c})] \\ \frac{d\theta}{dt} = -\frac{V}{D_c}[\theta + B\ln(\frac{V}{V_c})] \end{array}\right\} \tag{1}$$

where the friction stress τ is a function of the normal stress σ, μ_o is a constant coefficient of friction, D_c is the critical slip distance in order for friction to change from static to dynamic values [Rabinowicz, 1951] (D_c is also denoted in some formulations of these laws as L). V is the slip rate, V_c is a constant introduced for dimensional consistency [Ruina, 1983], A and B
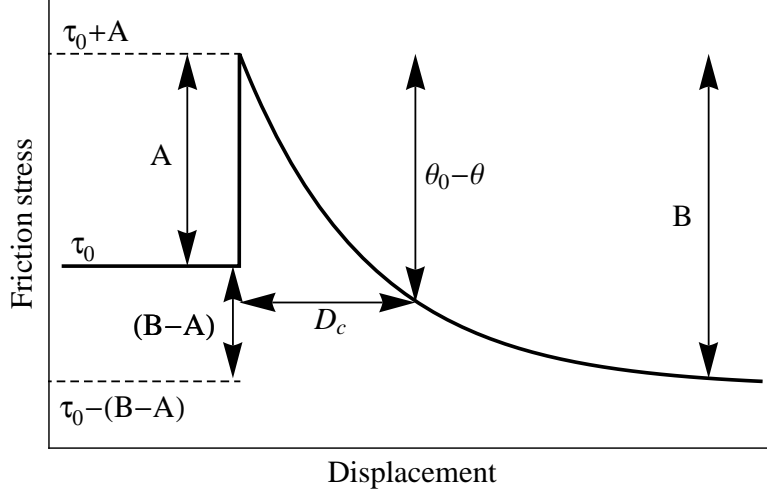
Figure 1: Schematic diagram taken from Erickson et al. [2008] (originally from Scholz [2002]), illustrating the response to a step change in the imposed velocity, v of a single spring-block slider model. The imposed velocity, initially maintained constant at v_0, is suddenly incremented by Δv and subsequently held constant at $v_0 + \Delta v$. The friction stress τ, initially constant at τ_0, suddenly increases to A when the velocity is incremented by Δv and then decreases exponentially to a new value B The length scale D_c (also known as L), characterizes the distance taken by the state variable θ to reach a new steady state θ_0.

are positive frictional parameters corresponding to the response to a step change in the imposed velocity of a single spring-block configuration [Scholz, 2002] (see Figure 1) and θ is the state variable. And while there are other formulations of the D-R friction law, and none can completely simulate all the laboratory data of friction, the studies conducted by Ampuero and Rubin [2007] (and references therein) suggest that the slip law is far more consistent with laboratory experiments.

According to Dieterich and Kilgore [1994], the parameter D_c corresponds to the critical sliding distance necessary to replace the population of asperity contacts. The parameters A and B are empirical constants, however the meaning of these two parameters is best understood by writing the expression for the friction stress:

$$\tau = \tau_0 + \theta + A \ln(v/v_0),$$

where τ_0 is the traction when the oscillator is moving at constant velocity v_0. When the slider moves at constant velocity v_{ss} (steady state), the expression for the stress becomes:

$$\tau_{ss} = \tau_0 - (B - A) \ln(v_{ss}/v_0).$$

According to Rice [1983] and Rice et al. [2001], the parameter $A = \partial \tau / \partial \ln(v)$ is a mea-
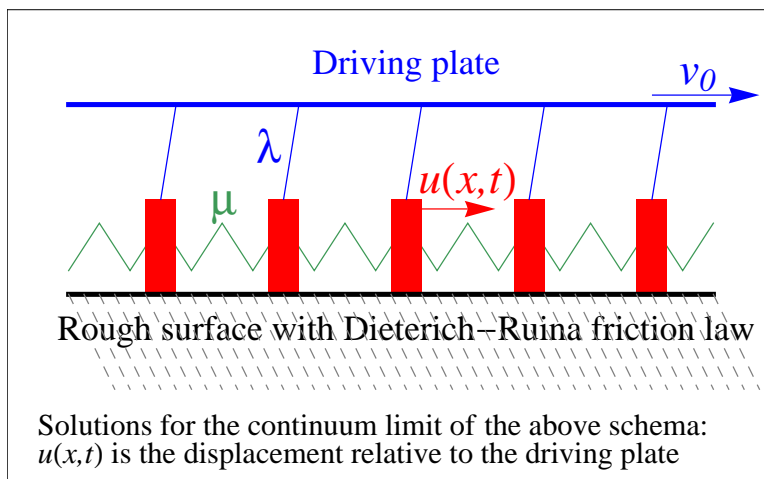
3

Figure 2: The equations of motion are derived from the dynamics of a spring connected chain of blocks, elastically coupled to a driver plate moving at a constant velocity V_0. $u(x, t)$ is the slip value for each block, μ is the spring coefficient between blocks and λ corresponds to the elastic coupling with the driver plate. The blocks slide along the rough surface determined by Dieterich-Ruina friction. Depending on the internal parameters, the chain will move in a variety of ways.

sure of the direct velocity dependence (sometimes called the "direct effect") while $(A - B) = \partial\tau_{ss}/\partial \ln(v_{ss})$ is a measure of the steady-state velocity dependence (see Figure 1). When compared to the slip weakening friction law, the parameter $(B - A)$ plays a role of a stress drop while A corresponds to the strength excess [Ohnaka and Shen, 1999]. Furthermore, A and B are related to the nondimensional seismic ratio introduced by Andrews [1976] in the following sense: $S = \frac{A}{B-A}$.

1.3   The Burridge-Knopoff Model

The ability of the D-R friction law to properly reproduce earthquake dynamics is studied by the formulation of a dynamic rupture model subject to a friction law, an initial spatial distribution of the stress and strength of the material over the fault surfaces, as well as a mathematical description of how these properties evolve during the rupture process. One type of dynamic model, studied extensively since its introduction in the 1960s, is the Burridge and Knopoff [1967] (BK) model of many blocks interconnected by elastic springs (see Figure 2) with spring stiffness coefficient μ. The blocks are also elastically coupled (with spring stiffness coefficient λ) to a rigid plate moving at a constant velocity V_o and pulled over a rough surface described by some friction law. The interface between the blocks and the rough surface can be considered an analogue for a 1-dimensional earthquake fault [Carlson et al., 1991]. Although there are more physical rupture models available (for a comprehensive review of numerical implementations

of dynamical modeling of earthquake rupture see Section 2 of Madariaga and Olsen [2002] and references therein), the Burridge-Knopoff model is more convenient as it allows us to simulate many scenarios of rupture without being too expensive in regard to computing time. Thus we have the ability to explore the parameter space of the system more broadly and observe the emergent dynamics introduced by the friction law.

Burridge and Knopoff [1967] conducted several laboratory experiments of this system - the first case considered equal spring constants between blocks, and the second with graduated values for the spring constants. They observed several types of behavior in this configuration including the presence of large shocks in the system when the spring constants were stretched far enough to set the blocks on the verge of instability. And while they found a Gutenberg-Richter distribution of event sizes present in their model, they note that statistical properties along the fault surface are determined by the nature of the friction law describing the interface (a property confirmed, at least partially, by Elbanna and Heaton [2009]). At this time rate and state friction laws had not yet emerged as powerful tools in dynamic simulations however. Burridge and Knopoff formulated the equations of motion for this system incorporating a friction law that was dependent only on the block's velocity.

These equations and similar formulations of them have been studied in detail since this time. In studies involving a velocity weakening friction law attached to a BK model, the internal parameter space has been explored and a rich variety of dynamics have been observed including chaotic regimes as well as localized solutions, see [Carlson et al., 1991] [Schmittbuhl et al., 1993], [Schmittbuhl et al., 1996], [Español, 1994], [Elbanna and Heaton, 2009]. Carlson and Langer [1989] considered a spring-block model under a velocity weakening friction law: if X_j is the position of the jth block then the friction acting on this particle is given by:

$$F(\dot{X}) = F_o\phi(\dot{X}/v_1), \tag{2}$$

where v_1 is a characteristic speed and ϕ vanishes for large values of $\dot{X}$ and is normalized so that $\phi(0) = -\phi'(0) = 1$. They found that this friction law exhibits periodic as well as stick-slip motion in the spring-block system. Furthermore, Carlson et al. [1991] found a transition from localized to delocalized events and derived a parameter condition for the BK model under velocity-weakening friction that guarantees that pulses remained sufficiently small so as not to propagate into the outer, firmly stuck regions in the model. In Schmittbuhl et al. [1993], the authors found a wide range of event types by varying a control parameter proportional to the product of the driving rate and the size of the system. The authors found that by increasing their parameter $\Theta = N \times v$, where N is the size of the system (number of blocks) and v is the driving displacement rate, a transition from chaotic to localized (solitary wave type) solutions occurred (referred to as a "finite-size effect"). When $\Theta = 8$, for example, a solitary wave emerged with

5

constant speed (10 blocks per time unit) and a wavelength of 8 blocks. Furthermore, the work of Español [1994] studied a Burridge-Knopoff model of a spring-block system subject to velocity weakening friction, namely

$$F(v) = \frac{F_o}{1 + \frac{v}{v_f}}, \tag{3}$$

where v_f is a characteristic velocity for friction and F_o is the threshold friction. In their model, the speed of sound, l is defined by the ratio of the spring constant between the blocks and the spring constant connecting the block to the driver plate: $l^2 = \frac{\mu}{\lambda}$. By varying the speed of sound, they observed intervals in which periodic, complex or localized, solitonic behavior emerged. For large values of l, they found periodic motion, while for intermediate values of l, they found various amounts of solitonic behavior, the pulse sometimes undergoing several turns in the chain of blocks before decaying.

It is important to note that chaotic behavior and localized events found in these studies consider a Burridge-Knopoff model under a different, nonlinear friction law (i.e. velocity weakening). Because we find similar behavior with the rate and state Dieterich-Ruina friction law, it introduces the question of whether or not the specific form of the friction law matters, or if the nonlinearity of the law alone is sufficient in generating these dynamics.

1.4 Modeling Challenges

Although the use of rate and state dependent friction is justified by empirical studies in the laboratory, there are disadvantages because of the difficulties that the nonlinearity of the D-R friction law imposes in the numerical simulations. As detailed in Erickson et al. [2008], the D-R friction law attached to dynamic models can result in differential equations that are very stiff in the numerical sense. Naïve methods to numerically integrate these equations are extremely inefficient and computationally expensive. For these reasons, the D-R friction law has often been altered in numerical simulations. Lapusta and Rice [2003] incorporated a regularized formulation of D-R friction in a 2-dimensional antiplane framework. However, for the parameter range they considered, they found only periodic behavior in their solutions. Either alteration of the nonlinear term or an insufficient exploration of parameter values may explain why chaotic regimes have rarely been observed with rate and state friction laws.

In addition to numerical difficulties, implementing a robust friction law in the dynamic model of an earthquake presents another fundamental challenge. Friction laws like the D-R friction law or the Free Volume law ([Daub and Carlson, 2008]) have been developed to describe the physical processes of small samples in laboratory experiments with a micro-scale lengths on the

order of the cm or less. Applications of these friction laws into numerical models of earthquakes will thus require making assumptions about the spatial properties of the parameters of the friction law as current numerical implementation of a dynamic model of an earthquake requires a description of the initial stress and the friction law at a length scale of the order of ~ 100m. It's possible that the emergent behavior from a full-scale rupture model can be lost or altered when considering models of this size, as modern computing capabilities prevent us from being able to prescribe frictional properties at the micro-scales in a full-scale model.

In addition to possible problems introduced by attaching laboratory derived friction laws to full scale models, dynamic modeling requires a correct description of the spatio-temporal variability of parameters involved in the earthquake rupture process. This makes the simulation of the propagation of the rupture and prediction of the ground motion possible. Unfortunately there has been little agreement on proper parameter values and our evidence to date suggests that a proper quantification of parameter values across the fault is neither achieved, nor well understood. For instance, the selection of the parameters values can be complicated when heating and pore pressure are included [Rice, 2006]. More generally, the proper question is to determine the spatial distribution of these parameters along the fault surface. Direct estimates of them into realistic conditions prevailing during an earthquake is currently unattainable and there is no evidence that indirect estimate of the parameters of the friction laws through inversion methods will lead to an important breakthrough. For instance, current attempts to determine the spatial variability of the slip-weakening distance D_c (a parameter common to several friction laws, including the D-R friction law) are inconclusive. Zhang et al. [2003] for example, found difficulties in the determination of values for D_c due to constraints in kinematic inversion and were able to estimate only an upper bound on values of D_c. Using a slip weakening friction law to compute the parameters of a dynamic rupture model, Peyrat et al. [2004] conclude, "it may not be possible to separate strength drop and D_c using rupture modeling with current bandwidth limitations". Using dynamic rupture inversion of a synthetic earthquake to compute the initial stress and D_c, Corish et al. [2007] can only estimate the average value of D_c. Furthermore, they conclude that "there is a trade-off between the average initial stress on the fault and the slip-weakening distance that precludes identification of the exact values of either quantity based on strong-motion records".

Although there lacks a strong consensus made for a proper regime of relevant parameter values, we develop the proper numerical methods capable of handling the numerical challenges introduced by the nonlinearity of the D-R friction law and are able to explore the parameter space quite deeply. This allows us to study the Burridge-Knopoff spring and block model subject to this friction law and analyze how each parameter influences the emergent behavior. This in turn sheds light on the parameter values capable of reproducing earthquake dynamics and may lead to a method for determining appropriate values to be used in future dynamic rupture simulations

7

with more sophisticated models.

2 The 1-Dimensional Discrete Model

2.1 Extension of the Single-Block Case

In Erickson et al. [2008] we conducted an in-depth study of the parameters associated with a BK model of single spring-block subject to the nonlinear D-R friction law and discussed its ability to capture 1-dimensional earthquake motion. We began numerical simulations of the model by using the version proposed by Madariaga [1998] of a single spring-block oscillator. In this form one can view the block's slip relative to the pulling force or driver plate. The equations of motion coupled with "slip-law" formulation of the Dieterich-Ruina rate and state dependent friction law (equation (1)) are given by:

$$\left.\begin{aligned}\dot{u} &= v - v_0 \\ \dot{v} &= (-1/M)[ku + \theta + A\ln(v/v_0))] \\ \dot{\theta} &= -(v/D_c)(\theta + B\ln(v/v_0))\end{aligned}\right\} \tag{4}$$

where u is the slip, v is the slip velocity, v_0 is a reference velocity and θ is the state variable. The parameter M is the mass of the block. In this context, the spring stiffness k corresponds to the linear elastic properties of the medium surrounding the fault [Scholz, 2002] and the parameters D_c, A, and B are the parameters of the D-R friction law described in section 1.2.

System (4) can be non-dimensionalized (see [Erickson et al., 2008] for details) into the following form:

$$\left.\begin{aligned}\dot{u} &= v - 1 \\ \dot{v} &= -\gamma^2[u + (1/\xi)(\theta + \ln(v))] \\ \dot{\theta} &= -v(\theta + (1+\epsilon)\ln(v))\end{aligned}\right\} \tag{5}$$

where u is now the slip of the block relative to the driver plate,

$$\xi = (kD_c)/A$$

is the nondimensional spring constant,

$$\gamma = \sqrt{k/M}(D_c/v_o)$$

8

is the nondimensional frequency and

$$\epsilon = (B - A)/A$$

measures the sensitivity of the velocity relaxation and is a ratio of the stress parameters in the D-R friction law. Although more information on A and B can be found in section 1.2 and in Scholz [2002], the analogy with earthquake motion is that the parameter ϵ is determined by the ratio of the amount of stress dropped during an earthquake, to the stress increase that accompanies a sudden change in fault velocity (see Figure 1). Furthermore, this ratio implies that $\epsilon = 1/S$, where S is the nondimensional seismic ratio [Andrews, 1976]. That a relationship between ϵ and S exists is important in light of the fact that an increase in ϵ (equivalent to a decrease in S) instigates a transition into chaotic behavior. We found that when varying the parameter ϵ in the single spring-block model under D-R friction causes the stationary state to undergo a Hopf bifurcation into a periodic orbit. After ϵ is further increased, the system period doubles into periodic orbits of 2, 4, 8 etc. After this period doubling cascade, the system reaches a chaotic state for critical values ϵ. Assuming that the friction law is responsible for the nonperiodic behavior of earthquake events (like the conclusions made by Carlson and Langer [1989]), then dynamic modeling requires that ϵ be in this chaotic regime.

In the case of a single block subject to Dieterich-Ruina friction, critical values of ϵ were quite large (≈ 11). Thus we extend this study to the case of many blocks, in order to see if chaos ensues for a wider parameter range including smaller values of ϵ. This information may give us insight into which features of the D-R friction law are preserved, lost or added when considering systems of larger size.

We begin by deriving the discrete formulation of the Burridge-Knopoff spring-block model subject to the nonlinear Dieterich-Ruina friction law. We find however, that in keeping ϵ fixed at the small value of 0.5, the discrete system (ODEs) exhibits both periodic and aperiodic motion, where the system's transition to chaos is size-dependent, i.e. how many blocks are considered. The chain undergoes periodic motion when less than 20 blocks are considered. Under the same system parameters however, the chain will undergo chaotic motion when 21 or more blocks are incorporated, although this transition depends on the parameters under consideration.

2.2   Equations of Motion

The following equations of motion are derived from a one-dimensional chain of spring-connected blocks elastically coupled and driven by a plate moving at a constant rate V_o. The blocks slide along a rough surface according to the nonlinear D-R friction law (see Figure 2) and the equations of motion for the jth block's position u_j are given by:

9

$$\left. \begin{array}{l} m\ddot{u}_j = \mu(u_{j+1} - 2u_j + u_{j-1}) - \lambda(u_j - V_o t) - F_j(\dot{u}_j, \theta_j) \\ F_j(\dot{u}_j, \theta_j) = \theta_j + A\ln(\dot{u}_j/V_o) \\ \dot{\theta}_j = -(\dot{u}_j/D_c)(\theta_j + B\ln(\dot{u}_j/V_o)) \end{array} \right\} \tag{6}$$

where F_j is the rate $\dot{u}_j$ and state θ_j D-R friction law from equation (1), μ is the spring constant coupling the blocks, λ is the spring constant coupling each block to the driver plate, and V_0, A, B and D_c are the associated frictional parameters, described in section 1. The spring constants μ and λ can be interpreted as the elastic properties across the medium, and are held constant with $\mu = \lambda$ for the studies in this section. u_j is the position of the jth block, or its slip from its initial starting position.

The variable u has two components: $u = u_{plate} + V_o t$ where u_{plate} is the block's slip relative to the driving plate, and $V_o t$ is the distance the plate has moved in t units of time. For our purposes, we redefine the variable u_j to be the jth block's slip from its adjacent point on the driver plate, resulting in the following equations:

$$\left. \begin{array}{l} m\ddot{u}_j = \mu(u_{j+1} - 2u_j + u_{j-1}) - \lambda u_j - F_j(\dot{u}_j, \theta_j) \\ F_j(\dot{u}_j, \theta_j) = \theta_j + A\ln(\frac{\dot{u}_j}{V_o} + 1) \\ \dot{\theta}_j = -((\dot{u}_j + V_o)/D_c)(\theta_j + B\ln(\frac{\dot{u}_j}{V_o} + 1)) \end{array} \right\} \tag{7}$$

where u_j is now the jth block's slip relative to the driver plate.

We non-dimensionalize the system in the manner of Madariaga [1998] (as described in Erickson et al. [2008]) then return to the use of θ, v, u and t. The non-dimensional equations are given by:

$$\left. \begin{array}{l} \ddot{u}_j = \gamma^2(u_{j-1} - 2u_j + u_{j+1}) - \tilde{\gamma}^2 u_j - (\gamma^2/\xi)(\theta_j + \ln(\dot{u}_j + 1)) \\ \dot{\theta}_j = -(\dot{u}_j + 1)(\theta_j + (1 + \epsilon)\ln(\dot{u}_j + 1)) \end{array} \right\} \tag{8}$$

where u_j is the non-dimensional slip of the jth block relative to the driver plate,

$$\gamma = \sqrt{\mu/m}(D_c/Vo) \text{ and}$$

$$\tilde{\gamma} = \sqrt{\lambda/m}(D_c/Vo)$$

are the nondimensional frequencies,

$$\xi = (\mu D_c)/A$$

10

is the nondimensional spring constant, and

$$\epsilon = (B - A)/A$$

as before (see section 1.2 and 2.1 for more information on ϵ, A and B).

2.3   Numerical Methods

Because of the nonlinearity imposed into equation (8) by the logarithmic term in the D-R friction law, analytic integration cannot be done even in the simplest case of a single block. For this reason we proceed by implementing a numerical method by first writing (8) as a system of 3 first order ODEs:

$$\left.\begin{aligned}
\dot{u}_j &= v_j \\
\dot{v}_j &= \gamma^2(u_{j-1} - 2u_j + u_{j+1}) - \tilde{\gamma}^2 u_j - (\gamma^2/\xi)(\theta_j + \ln(v_j + 1)) \\
\dot{\theta}_j &= -(v_j + 1)(\theta_j + (1 + \epsilon)\ln(v_j + 1))
\end{aligned}\right\} \qquad (9)$$

As mentioned in the previous section, Dieterich-Ruina friction has introduced numerical challenges because the nonlinearity of the logarithmic term causes the system's local Jacobian matrix to have very negative eigenvalues - a property that usually indicates the presence of numerical stiffness (well documented in [Erickson et al., 2008], [Noda et al., 2008], and [Rojas et al., 2009]) . During our simulations conducted in Erickson et al. [2008] we found that even with the use of an implicit numerical method suited for numerically stiff problems, the time step was still restricted by accuracy requirements. Even with a stable method, if the time step taken is too large, then the algorithm returns numerical value of $v_j < -1$ and the logarithmic term is undefined. For this reason, we use a classical fourth order explicit Runge-Kutta method on the ODEs in equation (9) whose step size adapts according to requirements for accurate resolution when v_j is close to -1.

N blocks are evenly spaced on a chain of length 20 dimensionless spatial units. Since fault rupture is caused by small stress instabilities along the fault surface and often propagate like a localized pulse [Heaton, 1990], we choose to represent the initial data as localized departure from the equilibrium (or stationary) regime. Therefore initial data is a smooth Gaussian pulse centered at the middle block:

$$u_0(j) = 1.5e^{\frac{-(x_j - 10)^2}{\sigma^2}}, \text{ for } j = 1, ...N, \text{ where } \sigma = 1,$$
$$v_0(j) = 0, \text{ for } j = 1, ...N$$

This corresponds to imposing an initial stress peturbation into the initial position of each block from its adjacent point on the driver plate, the middle block having the greatest initial displacement. All have zero initial velocity (with respect to the driver plate). Free boundary conditions

imply that blocks on either end of the chain are only influenced by the single block connecting them to the chain, and their elastic coupling with the driver plate.

2.4 Transition to Chaos

Because of a lack of insight into proper parameter values (explained in section 1.3), we explore the parameter space that allows for more manageable numerical computation (i.e. where the parameters associated with the nonlinear terms are not too large). Numerical integration is done for different amounts of blocks: $N = 3$, 10, 20, and 21 blocks. Parameter values used here are fixed at $\epsilon = 0.5$, $\xi = 0.5$, $\gamma = 0.5$ and $\tilde{\gamma} = 0.5$. Figures 3, 4, 5 and 6 correspond to different amounts of blocks considered. For each figure, the plot on the top left is the initial displacement of all N blocks and the top right is the slip of all N blocks against time. The plot on the bottom left is the contour of the middle block's slip against time and one can further view the periodic, or aperiodic behavior occurring. The bottom right plot is the phase space for the middle block's slip, velocity and state variable. Periodic orbits will appear as a single closed loop in the phase space, while aperiodic orbits will appear as a strange attractor (see [Erickson et al., 2008] for more explanation).

Figure 3 shows the results from a system of 3 connected blocks. After a transient period in which the initial perturbation is amplified, the nonlinearities saturate this growth and the system settles into the same periodic trajectory - suggesting that the blocks move collectively. All 3 blocks undergo abrupt, periodic motion of period approximately 20 temporal units and amplitude approximately 4 slip units. They are stuck to the rough surface until the driver plate overcomes the static friction holding each block in place, and the chain suddenly begins to slide. After a time period, the blocks approach a gradual stop until the pulling force overcomes static friction, and the cycle begins again. Sudden and jerky motion, reminiscent of stick-slip behavior emerges as the blocks respond to the driver plate. Under the same parameter combination, periodic motion occurs when considering the system of 10 blocks as viewed in Figure 4, although it appears that the period of the solution has undergone at least one period doubling bifurcation. In this case all 10 blocks undergo periodic motion, but their slip values reach different amplitudes - the block in the center of the chain reaches an amplitude of approximately 3 slip units during each cycle, while nearby blocks reach smaller amplitudes. Similar is the case for $N= 20$ blocks, although the periodicity of the motion appears to double again.

For this fixed set of parameter values, the motion is periodic in time for $N = 3,...,20$, but when $N = 21$, the motion becomes aperiodic in time. As seen in Figure 6, each block follows its own chaotic trajectory in time and the blocks appear to move independently of each other - suggesting chaotic behavior in space as well. Further studies show that this transition to chaotic motion varies, depending on the parameters considered. More specifically, the fact that a tran-
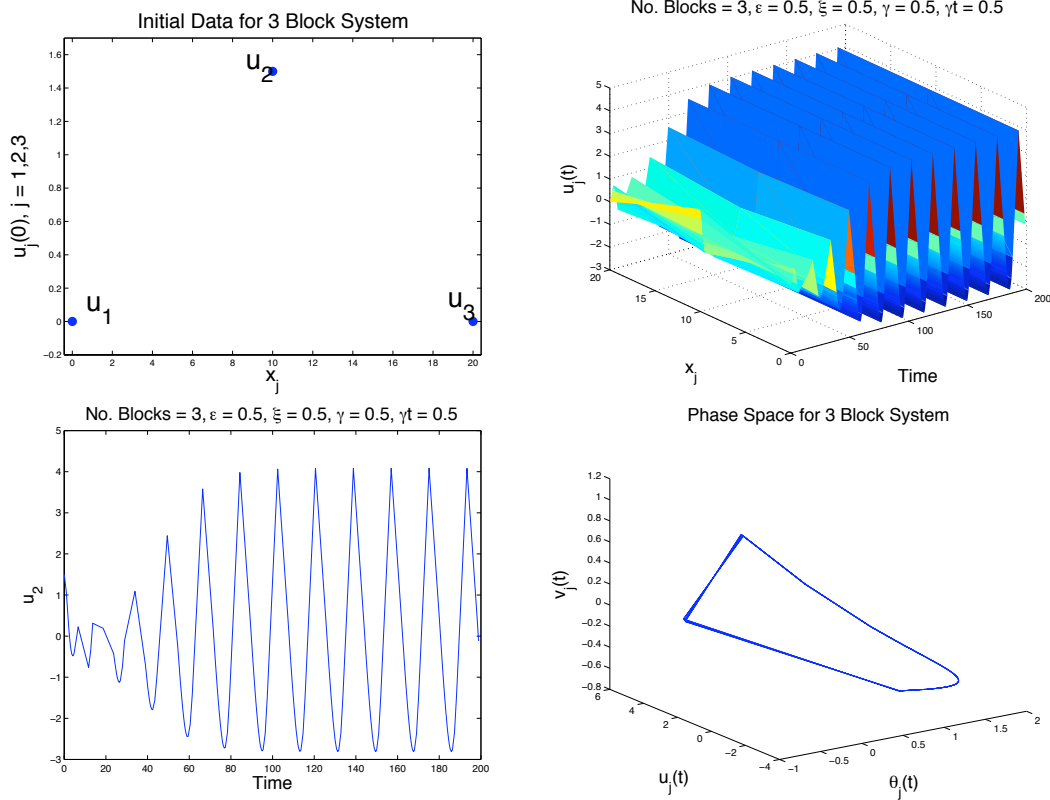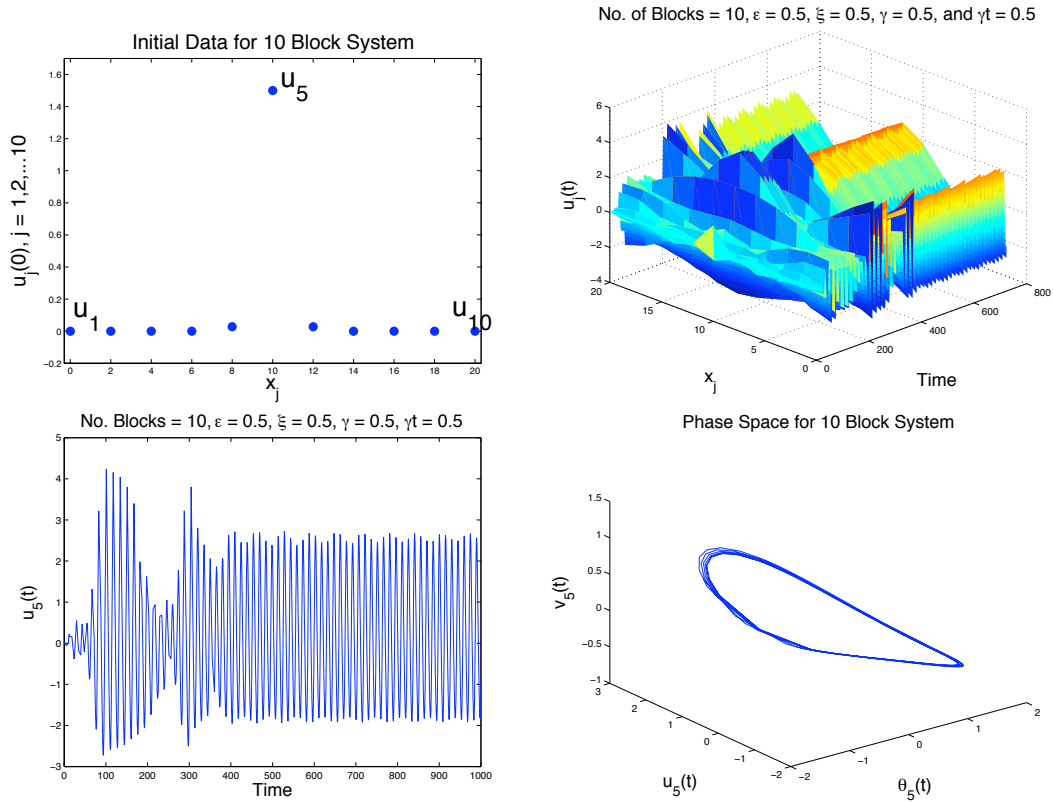
Figure 3: Solution to the ODEs derived from a 3 block system. The top left figure shows the initial data, where the boundary conditions fix the two end blocks at zero displacement, and the center block is displaced by a value from smooth Gaussian distribution. The top right plot shows the slip of all 3 blocks against time and the motion is periodic in time, each block attaining the same amplitude. The bottom left figure shows the slip of the middle block against time, where an initial transient period exists during which the small instabilities introduced by the initial slip displacement are amplified, then saturated by the system's nonlinearities and then settle into periodic motion. The bottom right plot shows the middle block's slip, velocity and state variable value in the phase space. These bottom two plots emphasize the periodic motion that this block undergoes.
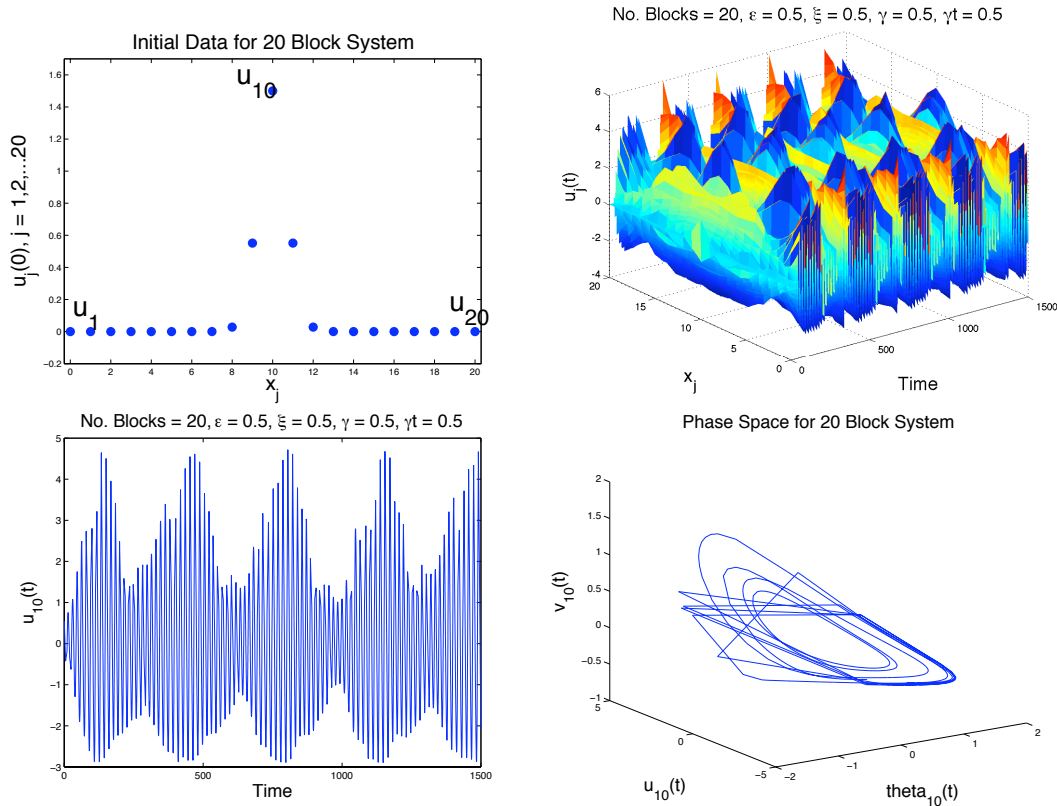
Figure 4: Solution to the ODEs derived from a 10 block system. The top left figure shows the initial data, where the boundary conditions fix the two end blocks at zero displacement, and the center blocks are assigned initial displacements from a smooth Gaussian distribution. The top right plot shows the slip of all 10 blocks against time and after a transient period, the chain settles into what appears to be periodic motion. The blocks reach different amplitudes, the center block and blocks near the end reaching an amplitude of about 3 units, while the remaining blocks reach smaller amplitudes. The bottom left figure shows the slip of the center (fifth) block against time, where an initial transient period exists during which the small instabilities introduced by the initial slip displacement are amplified, then saturated by the system's nonlinearities and then settle into periodic motion. The bottom right plot shows the center block's slip, velocity and state variable value in the phase space. These bottom two plots emphasize the periodic motion that this block undergoes.
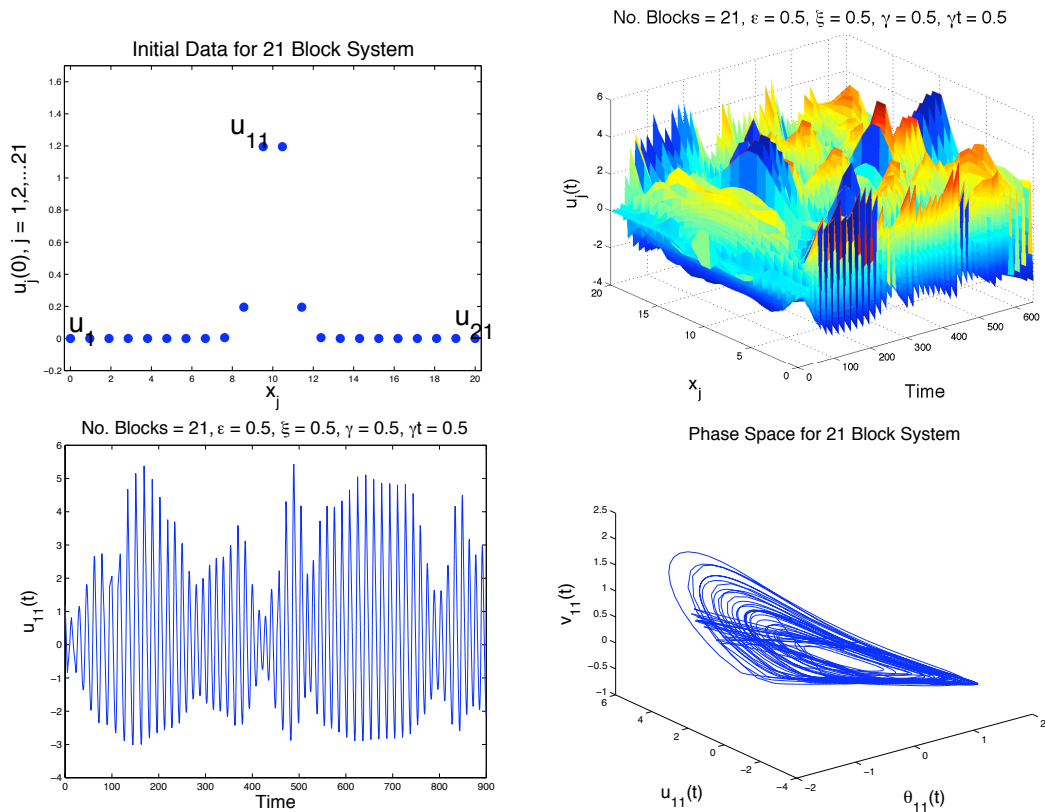
Figure 5: Solution to the ODEs derived from a 20 block system. The top left figure shows the initial data, where the boundary conditions fix the two end blocks at zero displacement, and the center blocks are assigned initial displacements from a smooth Gaussian distribution. The top right plot shows the slip of all 20 blocks against time and after a transient period, the chain settles in to what appear to be periodic motion. The blocks reach different amplitudes, the center block and blocks near the end reaching an amplitude of almost 5 units, while the remaining blocks reach smaller amplitudes. The bottom left figure shows the slip of the center (tenth) block against time, where an initial transient period exists during which the small instabilities introduced by the initial slip displacement are amplified, then saturated by the system's nonlinearities and then settle into periodic motion. The bottom right plot shows the center block's slip, velocity and state variable value in the phase space. These bottom two plots emphasize the periodic motion that this block undergoes.

15

Figure 6: Solution to the ODEs derived from a 21 block system. The top left figure shows the initial data, where the boundary conditions fix the two end blocks at zero displacement, and the center blocks are assigned initial displacements from a smooth Gaussian distribution. The top right plot shows the slip of all 21 blocks against time and maintains what appears to be chaotic motion. The bottom left figure shows the slip of the eleventh block against time, where an initial transient period exists during which the small instabilities introduced by the initial slip displacement are amplified, then saturated by the system's nonlinearities and then continue in aperiodic motion. The bottom right plot shows the center block's slip, velocity and state variable value in the phase space. These bottom two plots emphasize the chaotic motion that this block undergoes.

16

sition occurs between $N = 20$ and $N = 21$ is not universal; it depends on the parameters used. It is also important to note that regardless of the type of motion these systems produce, one can observe from Figures 3, 4, 5, and 6 that there is a transient period during which small instabilities introduced by the initial slip displacement is amplified as energy enters the system. This amplification is then saturated by the nonlinearities present from the friction law. This feature suggests that under these parameter values, the friction law can be a mechanism responsible for causing even small instabilities to grow into large, but finite events, similar to the conclusions made by Carlson and Langer [1989] who stated that the velocity weakening friction law was responsible for the amplification of small heterogeneities in the initial spatial distribution, leading to chaotic motion.

It should also be noted that in addition to an initial transient region and a chaotic regime, the system of 21 blocks tend to synchronize and move in periodic motion - although this is only after a long time in the chaotic state and it's possible that this behavior only occurs for the parameter values we considered. The initial transient region seems to depend on the number of blocks considered. In the case of 3 blocks (see Figure 3) the transient region in which the initial data is amplified lasts up until $T_1 \approx 50$, whereas this time is $T_1 \approx 100$ in the case of 10 or 20 blocks. After a period in the transient regime, the systems of 3, 10 or 20 blocks enter a periodic regime. However, in the case of 21 blocks, after a transient regime in which the initial data is amplified (also lasting until $T_1 \approx 100$), the systems enter a chaotic state that lasts until $T_2 \approx 800$, before synchronization sets in and the system enters a periodic regime. The ratio of time spent in the transient regime to time spent in the chaotic regime, $\frac{T_1}{T_2}$ is therefore approximately $\frac{1}{8}$. These numbers are only a rough estimate however, and may vary if different parameter values are considered.

Further insight into these solutions is gained by computing the Fourier power spectrum (see [Erickson et al., 2008] for details on how the power spectrum is computed) as viewed in Figure 7. We consider the middle block in each chain of length 3, 10, 20 and 21 blocks. Figure 7 shows the power spectrum (normalized with respect to the fundamental frequency) for the system of 3, 10, 20 and 21 blocks, and one can further view the periodic or aperiodic motion of these systems. The power spectrum for 20 blocks however, shows its power concentrated at the dominant frequency and its harmonics. The last plot in Figure 7 shows the power spectrum for the system of 21 blocks, where broadband noise is present, suggesting chaotic motion.

We can view the aperiodic behavior in the power spectrum in more detail by plotting the log-linear plot of the power against the frequency. Figure 8 shows this data for the chaotic solutions from the 21 block system. We see that the spectra for this system experiences two regimes of decay. There is an initial period where the power spectrum undergoes exponential decay which is then followed by slower, algebraic (power-law) decay. Sigeti [1995] acknowledges the common agreement that the power spectra computed from continuous-time dynamical systems within the
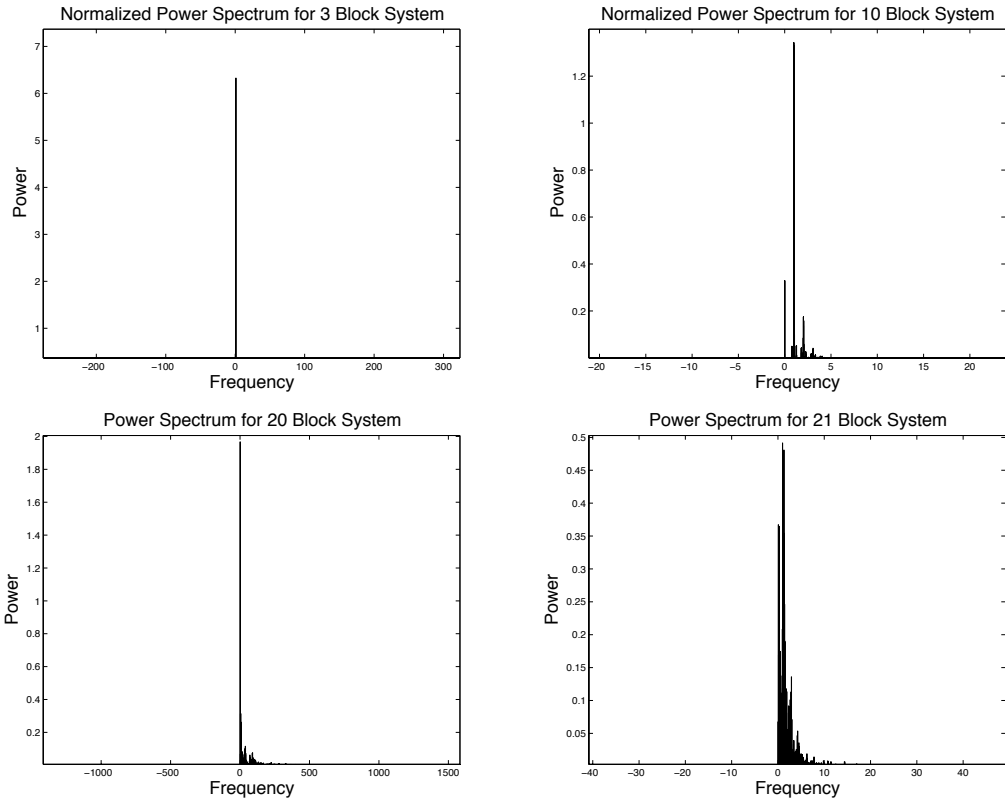
Figure 7: Normalized power spectra for the slip associated with 3, 10, 20 and 21 blocks. The single peak in the first plot further emphasizes the period 1 behavior of the solutions to the model when considering 3 blocks. The second two plots suggest the periodic behavior of the systems of 10 and 20 blocks. Each plot reveals a finite amount of peaks, with 1 or 2 strong peaks and several harmonics. The last plot shows the normalized power spectra for the slip associated with 21 blocks where a transition to chaos occurs, as broadband noise is evidenced by the high number of frequencies represented.

18
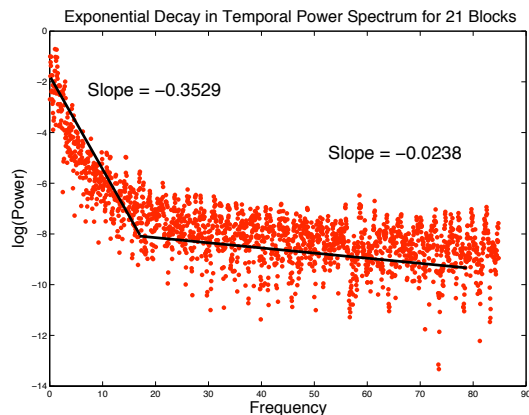
Figure 8: The log-linear plot for power against frequency for the systems of 21 blocks shows two regimes of decay. For both systems we see an initial period where the power spectrum experiences exponential decay, but this is followed by slower, algebraic (power-law) decay.

chaotic regime experience exponential decay. That this is followed by a second regime in which a power-law behavior is present has also been seen in several dynamical systems that exhibit chaos, like those documented in Valsakumar et al. [1997]. The power law behavior is a feature not uncommon to many areas of geology and geophysics and evidence of a fractal distribution (see [Turcotte, 1997] and references therein). For instance, the well known Gutenberg-Richter law for frequency-magnitude earthquake distribution follows a power law, as does topography [Turcotte, 1997] and turbulent flow [Frisch, 1995].

3 The Continuum Formulation

3.1 Extension of the Discrete Model

As we have seen in the previous chapter, chaotic dynamics emerge in the discrete formulation when the number of blocks is increased. For this reason, we are interested in studying the dynamics of a continuum model to see if the behavior undergoes qualitative changes when considering infinitely many blocks. In this section we derive the nonlinear Dieterich-Ruina wave equation derived from the Burridge-Knopoff spring block system subject to the D-R friction law. We find that a transition to chaos also occurs when varying the parameter ϵ, similar to what we found in Erickson et al. [2008] for the case of a single block. The critical value of ϵ however, is much smaller than that required for a single block.

19

3.2 Equations of Motion

We can derive a continuous model for a chain of blocks by taking the continuum limit in the manner of Carlson and Langer [1989]. We let Δx be the distance between blocks so that the ratio $\frac{m}{\Delta x}$ is the mass per unit length of string, or linear density [Pain, 1968]. Then we consider equations (7) and (8) when $m, \Delta x \to 0$ and the additional rescaling: $x = D_c \hat{x}$. This yields our final equations of motion, given by the following elastic wave equation for $u(x, t)$ driven by Dieterich-Ruina friction and its associated state variable evolution equation:

$$\left. \begin{array}{l} u_{tt} = c^2 u_{xx} - \tilde{\gamma}^2 u - (\gamma^2/\xi)(\theta + \ln(u_t + 1))) \\ \theta_t = -(u_t + 1)(\theta + (1 + \epsilon) \ln(u_t + 1)) \end{array} \right\} \tag{10}$$

where the final equations now involve a fourth internal parameter:

$$c^2 = \lim_{m, \Delta x \to 0} (\mu D_c^2 \Delta x^2)/(m V_o^2)$$

the square of the wave speed, and ϵ, γ, $\tilde{\gamma}$ and ξ are defined in section 2.2.

3.3 Numerical Methods

To solve equation (10) numerically, we first write it as a system of 3 first order equations in time:

$$\left. \begin{array}{l} u_t = v \\ v_t = c^2 u_{xx} - \tilde{\gamma}^2 u - (\gamma^2/\xi)(\theta + \ln(v + 1))) \\ \theta_t = -(v + 1)(\theta + (1 + \epsilon) \ln(v + 1)) \end{array} \right\} \tag{11}$$

To approximate the spatial derivative u_{xx} we discretize in space using the method of lines [Ascher and Petzold, 1998]. This procedure approximates spatial derivatives with finite differences and yields a system of ordinary differential equations, the number of equations dependent on the spatial discretization. We chose to discretize the interval $x \in [0, 20]$ into $M = 200$ grid points, resulting in 200 ordinary differential equations and assigned the continuous version of the same initial slip as the discrete system in section 2, with zero initial velocity, namely

$$u(x, 0) = 1.5 e^{\frac{-(x-10)^2}{\sigma^2}}, \text{ where } \sigma = 1,$$
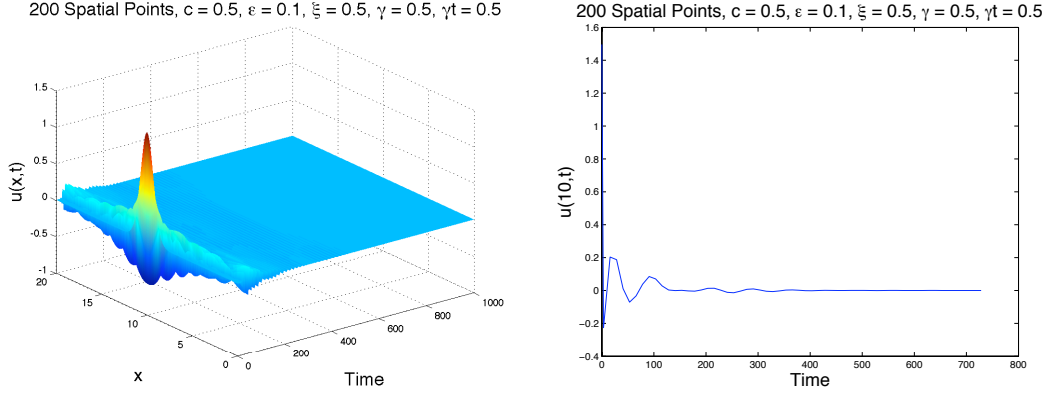$$v(x, 0) = 0,$$

20

Figure 9: Parameter combination $(c, \epsilon, \xi, \gamma, \tilde{\gamma}) = (0.5, 0.1, 0.5, 0.5, 0.5)$ yields a stationary solution to the PDE (10). Given a gaussian centered displacement for initial data, the slip of each point in space is slightly displaced from their adjacent points on the driver plate. During the initial transient region, the slip increases as the chain is pulled forward by the driver plate but each point along the chain responds differently due to the different friction forces acting on point along the chain. But after this time, the entire chain settles on its adjacent position to the driver plate, and the entire chain slides along at a constant rate with the moving plate. Thus relative slip values become zero and the velocity is constant.

and free boundary conditions as before. As mentioned in the previous section, this form of the initial data was chosen to represent localized departure from the equilibrium position and corresponds to slightly displacing the center of the continuum of blocks.

The method of lines is applied to the spatial derivative u_{xx} in (11) yielding the following system of ODEs:

$$
\frac{d}{dt}
\begin{bmatrix}
v_0 \\ v_1 \\ \cdot \\ \cdot \\ v_i \\ \cdot \\ \cdot \\ \cdot \\ v_M
\end{bmatrix}
=
\begin{bmatrix}
\beta & \alpha & & \alpha & & & & & \\
\alpha & \beta & \alpha & & \alpha & & & & \\
& \cdot & \cdot & \cdot & & \cdot & & & \\
& & \cdot & \cdot & \cdot & & \cdot & & \\
& \alpha & & \alpha & \beta & \alpha & & \alpha & \\
& & \cdot & & \cdot & \cdot & \cdot & & \cdot \\
& & & \cdot & & \cdot & \cdot & \cdot & \\
& & & & \cdot & & \cdot & \cdot & \cdot \\
& & & & & \alpha & & \alpha & \beta
\end{bmatrix}
\begin{bmatrix}
u_0 \\ u_1 \\ \cdot \\ \cdot \\ u_i \\ \cdot \\ \cdot \\ \cdot \\ u_M
\end{bmatrix}
- \frac{\gamma^2}{\xi}
\begin{bmatrix}
\theta_0 + \log(v_0 + 1) \\
\theta_1 + \log(v_1 + 1) \\
\cdot \\
\cdot \\
\theta_i + \log(v_i + 1) \\
\cdot \\
\cdot \\
\cdot \\
\theta_M + \log(v_M + 1)
\end{bmatrix},
$$

where $\alpha = \frac{c^2}{\Delta x^2}$, $\beta = -2\frac{c^2}{\Delta x^2} - \tilde{\gamma}^2$, and $M = 200$ (in this study) is the number of spatial points in the discretization. Due to such a large system of ODEs, we solved them in parallel, using a similar Runge-Kutta scheme as discussed in section 2 (for a summary of the parallel methods developed, see [Erickson, 2010]). With the goal in mind of answering whether or not the features of the D-R friction law are scale-dependent, we study the critical values of ϵ that lead to aperiodic behavior in order to see if the transition to chaos occurs for smaller values.
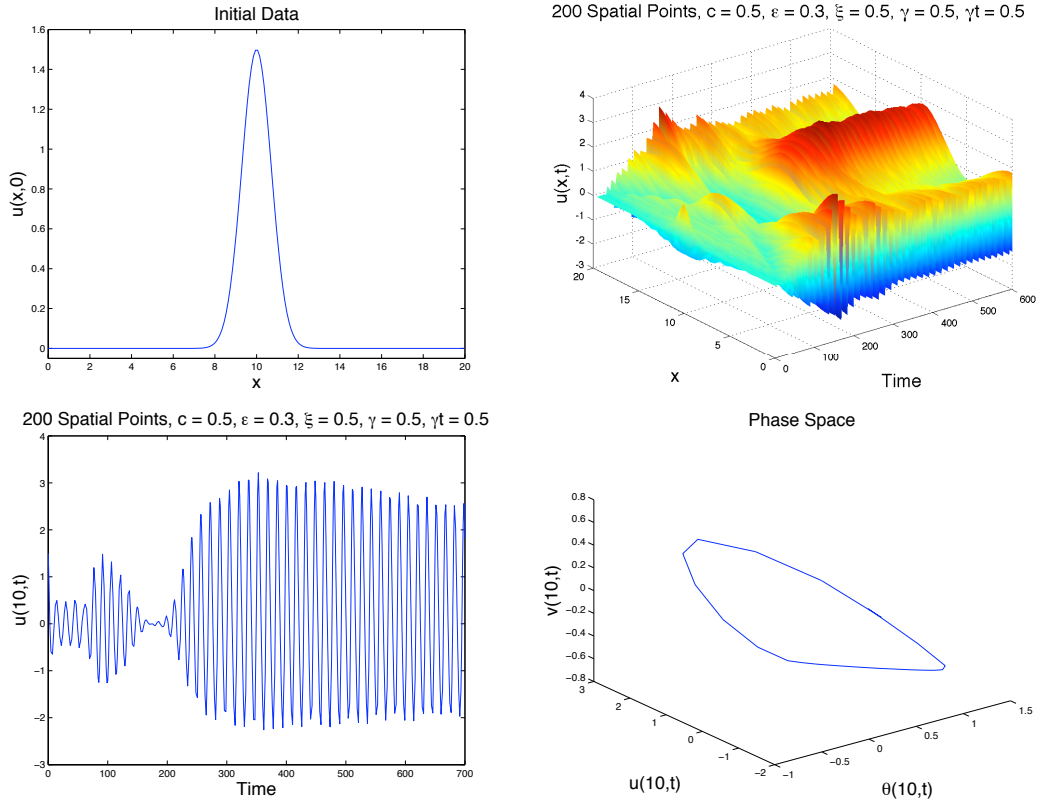
21

Figure 10: Parameter combination $(c, \epsilon, \xi, \gamma, \tilde{\gamma}) = (0.5, 0.3, 0.5, 0.5, 0.5)$ yields a periodic solution to the PDE in equation (10). Given the same initial displacement as in Figures 9 we observe that an increase in ϵ from 0.1 to 0.2 yields a bifurcation of the stationary state. During the initial transient region, the blocks are pulled forward by the driver plate but, due to the different friction forces acting on each block, respond differently in how far they slip. But after this time, each block settles on a periodic response to the driver plate, alternating between sliding and slowing down in response to the pull of the driver plate, and the roughness of the surface.
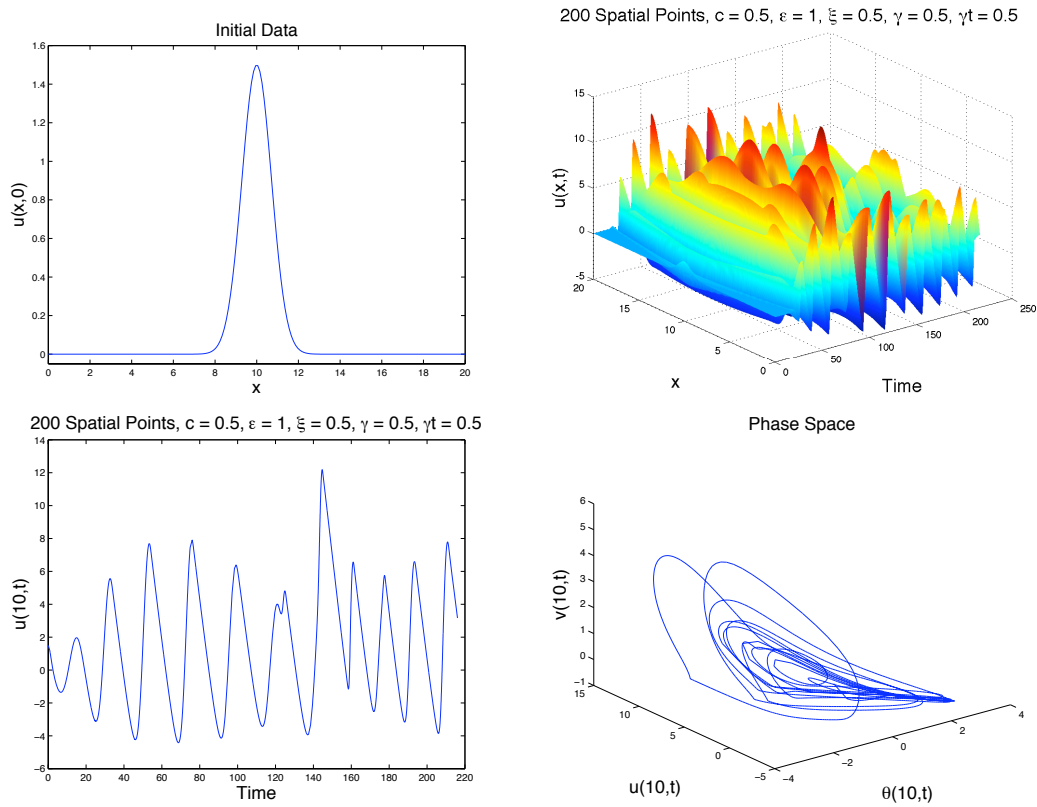
Figure 11: Parameter combination $(c, \epsilon, \xi, \gamma, \tilde{\gamma}) = (0.5, 1, 0.5, 0.5, 0.5)$ yields an aperiodic solution to the PDE in eqution (10). Given the same initial data as before (see Figures 9 and 10), the blocks are slightly displaced from their adjacent points on the driver plate. The parameter ϵ has been increased from 0.2 (periodic motion) to 0.5. During the initial transient region, the blocks are pulled forward by the driver plate but respond chaotically to the forces acting on them. Each point in space appears to undergo independent aperiodic motion - suggesting the presence of spatial as well as temporal chaos.

3.4 Transition to Chaos

Parameter combination $(c, \epsilon, \xi, \gamma, \tilde{\gamma}) = (0.5, 0.1, 0.5, 0.5, 0.5)$ yields a stationary solution as seen in Figure 9. The perturbation introduced from the initial displacement is amplified as the chain is pulled forward by the driver plate during an initial transient period. Because the friction along the surface is a function of each point's velocity $v(x, t)$ and asperity contact $\theta(x, t)$, each point responds differently in how far it slips. The center of the chain slips the greatest amount, relative to the driver plate, while the points near the ends of the chain remain almost stationary (sliding steadily with the driver plate). When the initial slip amplification is saturated by the nonlinearities, each point settles on its adjacent position to the driver plate, and the whole chain slides along at a constant rate with the moving plate. Thus relative slip values become zero, and all points slide with a constant velocity.

A bifurcation of this stationary state occurs when ϵ is increased from 0.1 to 0.2, as viewed in Figure 10 where a periodic solution emerges. After a transient period, the chain oscillates between negative and positive slip values; the point in the center attaining the most extreme values. Negative slip values correspond to the driver plate moving beyond the chain, while positive slip values mean points on the chain are slipping beyond the driver plate. The smoothness in the dynamics represents a fluid-like interaction between each point along the chain and the rough surface it slides upon. The chain fluctuates gently in response to the driver plate and the friction on the surface, approaching a full stop before sliding forward again.

For $\epsilon = 1$, chaotic motion appears in Figure 11 and one can see each point along the chain undergoing its own aperiodic motion as waves of different amplitudes propagate through the medium and interact with the boundary. Each point in space follows its own aperiodic trajectory - suggesting the presence of spatial as well as temporal chaos.

We can view these periodic and aperiodic solutions further by computing the associated power spectra, as shown in Figure 12. The top two plots are associated with the periodic solution viewed in Figure 10. The top left plot is that of the normalized temporal power spectrum, showing what appears to be 2 dominant frequencies surrounded by small harmonics. On the top right is its spatial power spectrum where periodic behavior is also visible. The bottom two plots further emphasize the chaotic behavior seen in Figure 11 as both show peaks at many frequencies. To view the power spectra more deeply we plot the log-linear plot of the power against the frequency. The plot in Figure 13 shows the decay of the power spectra for the chaotic solution to the PDE in equation (10) experiencing exponential decay for a short time period, before leveling off and decaying as a power law (algebraic decay). See section 2.4 for more on this type of behavior.
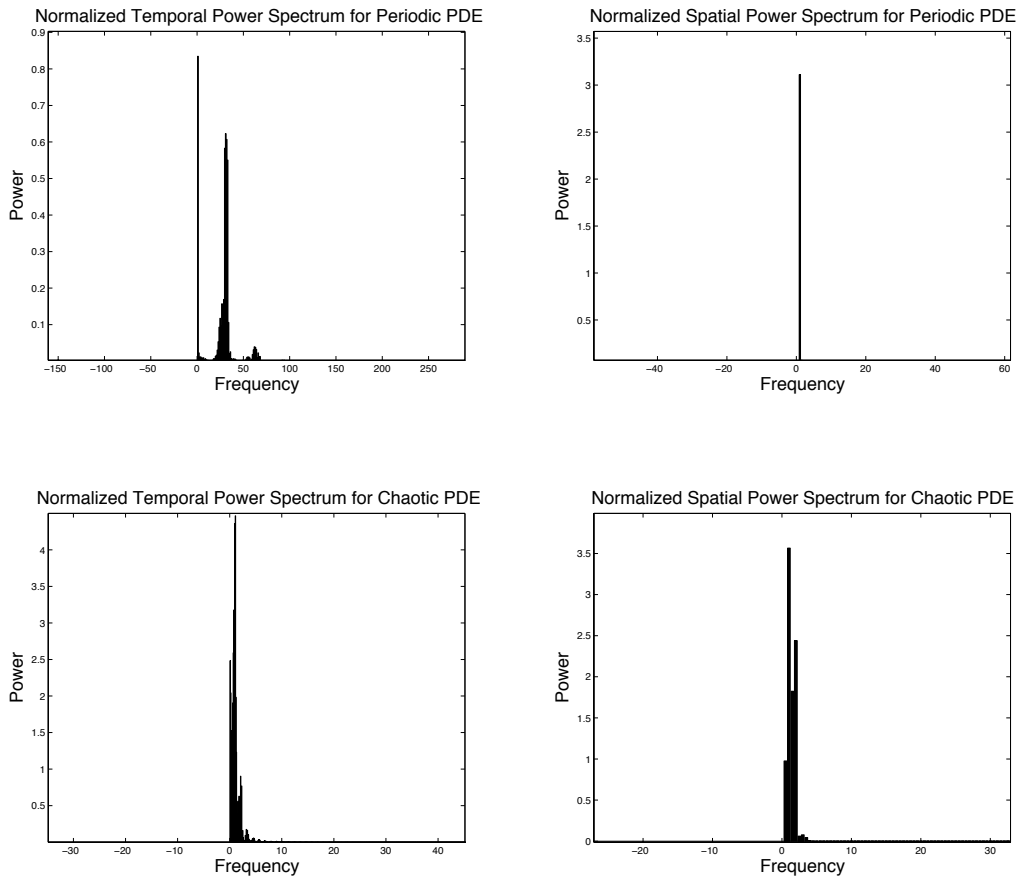
24

Figure 12: Normalized power spectra for periodic and aperiodic solutions to the PDE in equation (10). The top two plots correspond to the periodic solution shown in Figure 10. On the left is the temporal power spectrum, showing what appears to be 2 dominant frequencies with small harmonics clustering about them, suggesting period 2 behavior. On the right is the spatial power spectrum, clearly showing 1 peak corresponding to period 1 behavior. Thus there is neither temporal nor spatial chaos. The bottom two plots correspond to the chaotic solution show in Figure 11. On the left is the temporal power spectrum showing many high peaks and clusters of harmonics. On the right, a similar spread of frequencies occur, suggesting chaos in both time and space.
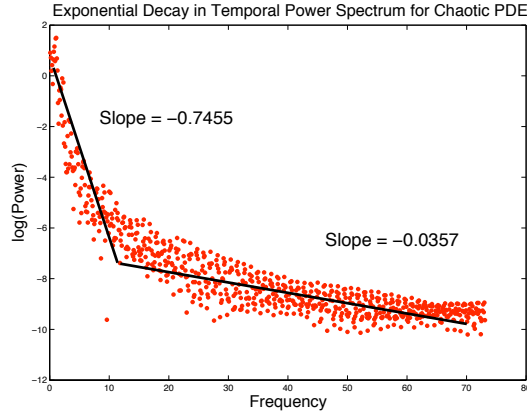
Figure 13: The log-linear plot for power against frequency for the chaotic solution to the PDE in equation (10) shows two regimes of decay. We see an initial period where the power spectrum experiences exponential decay, but this is followed by slower, algebraic (power-law) decay.

4 Localized Solutions

4.1 Solitons and Breathers

During the studies conducted in sections 2 and 3, we also observed that in certain parameter regimes both the discrete and the continuous formulations of the Burridge-Knopoff model subject to Dieterich-Ruina friction exhibit solutions where initial slip pulses remain localized in space. Like the studies of Español [1994] who studied a BK model with velocity weakening friction, we also found solutions that propagate like a traveling wave, or remain localized in space. The localized solutions suggest the presence of solitonic behavior, where initial data in the form of a smooth Gaussian pulse tends to remain localized under certain parameter values. In the case of a traveling wave we see evidence of a soliton, a solitary wave that maintains its shape while it travels at a constant speed through the medium. The solutions that remain localized in space and oscillate in time however, are known as breathers.

The general definition of a soliton solution to a nonlinear wave equation is that it has 3 properties: it is a wave with permanent form, that is localized in space for each fixed point in time, and if two solitons meet, their forms are preserved after the interaction [Mickens, 2004]. A breather, on the other hand, is a time-periodic, exponentially decaying (in space) solution of a nonlinear wave equation [Kichenassamy, 1991]. Breather solutions are rare and the only nonlinear wave equation known to possess large breather solutions is the sine-Gordon equation (see [Birnir, 1994], [Birnir et al., 1994] and references therein).

26

4.2 Significance of Localized Solutions

The significance of these types of solitary wave solutions was emphasized by Heaton [1990], who studied dislocation time histories generated from models derived from earthquake waveforms. He found that, contrary to crack-like dynamic rupture models where the rise time was comparable to the entire duration of rupture along the fault, dislocation rise times were only about 10% of the overall rupture duration. The most appropriate explanation for this observation of short slip durations is that the rupture travels like a self healing pulse that propagates along the fault. Heaton suggests that a dynamic friction law (he considers a law that is inversely related to slip velocity) can be a mechanism for causing the fault to heal itself shortly after the rupture passes through, resulting in a localized pulse. The rest of this section is devoted to the exploration the space of parameter values for which these types of soliton or breather solutions emerge for the nonlinear wave equation with D-R friction, equation (10). These solutions can be understood as a proxy for the propagation of the rupture front across the fault surface during an earthquake and may determine a range for suitable parameter values to be used in dynamic modeling of earthquakes.

4.3 Localized Solutions to Discrete and Continuous Formulation

As detailed in the introduction, Schmittbuhl et al. [1993] and Español [1994] observed (among others) solitary wave-type solutions when varying different parameters of the BK model subject to a velocity weakening friction law. Similar to the discoveries described in these papers, we have also seen solitary wave and localized solutions in both the discrete and the continuous models under the D-R friction law. Figures 14 and 15 show solutions from the ODEs and the PDE under similar conditions, where solitary, localized or unlocalized behavior emerges. Initial data is assigned to both of our systems in the form of a smooth Gaussian pulse with zero initial velocity namely,

$$u(x,0) = .01e^{(-(x-10)^2/\sigma^2)}, \text{ where } \sigma = 1,$$
$$v(x,0) = 0,$$

and free boundary conditions as before. This initial, localized pulse is again intended to represent localized departure from equilibrium and it tends to remain localized under certain parameter values, suggesting the presence of solitonic or breather solutions. We are interested in determining the parameter(s) on which this behavior depends.

In the next section we find that solitary and localized behavior seems to be dependent on the ratio between the parameters $\tilde{\gamma} = \sqrt{\lambda/m}(D_c/Vo)$ and $\gamma = \sqrt{\mu/m}(D_c/Vo)$, indicating that
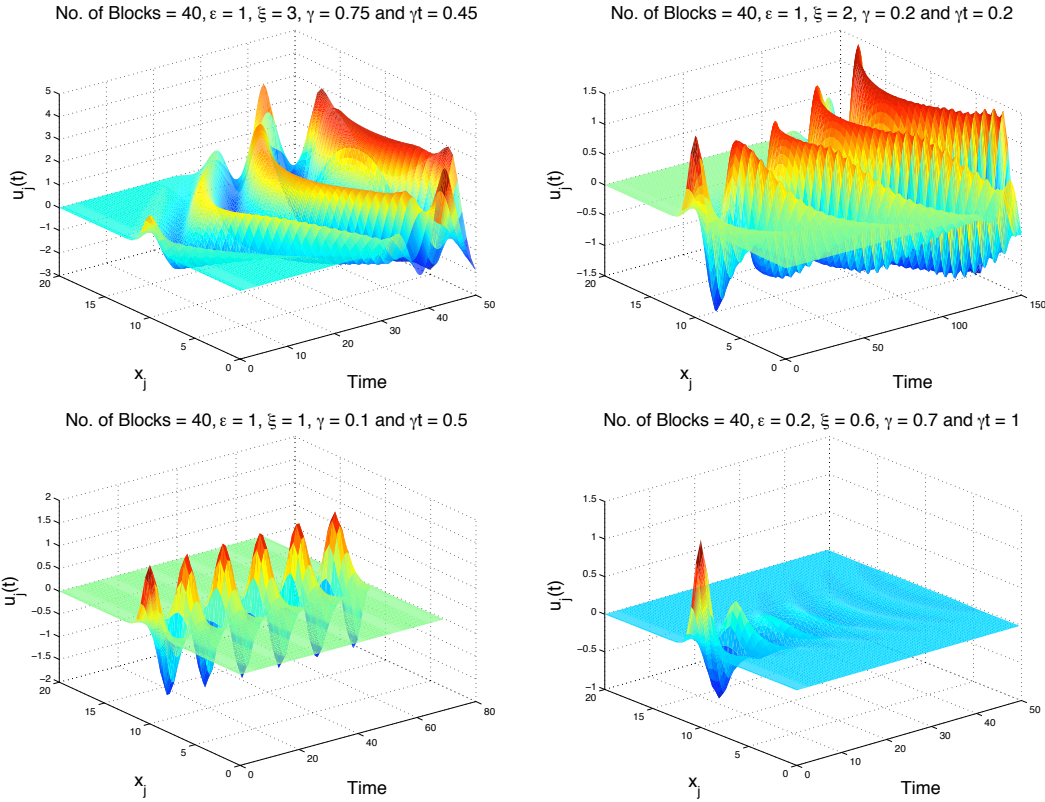
Figure 14: These four plots show the slip of a chain of 20 blocks with different parameter combinations. The parameters ϵ and ξ are fixed, while γ and $\tilde{\gamma}$ are varied. The top right plot shows that not all parameter combinations yield solitary or localized solutions, as we see the initial pulse split into two waves that travel quickly through the medium and interact with the boundary. The bottom two figures however, show solutions to the ODE system where the slip remains localized in space and the amplitude either remains at a constant height, or dies out. This suggests that both γ and $\tilde{\gamma}$ may be responsible for the localization, but that γ is probably responsible for causing the slip the die out (as $\tilde{\gamma}$ remains constant in the bottom two plots). The plot on the bottom right suggests that under these parameter values, the friction law alone can be a mechanism to halt rupture propagation.
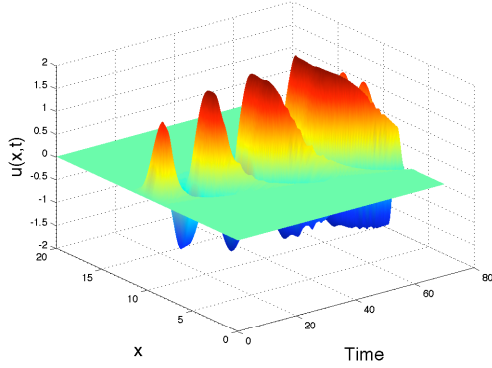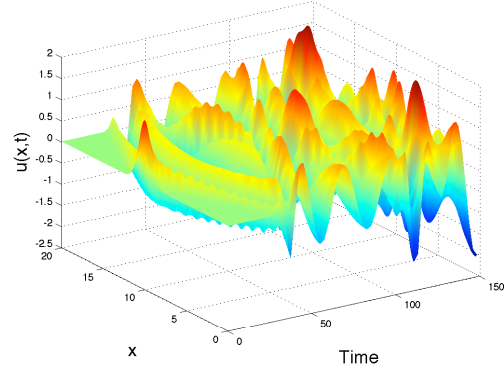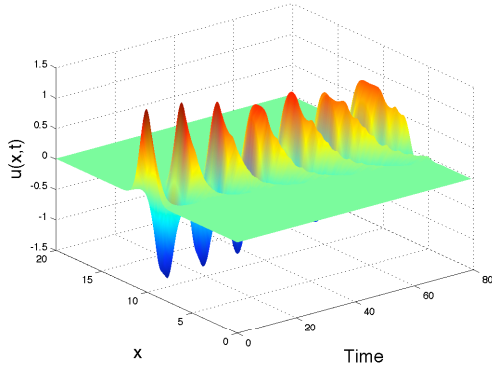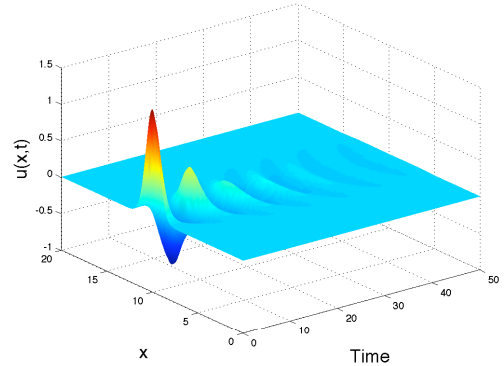
Figure 15: These four plots are the solutions to the PDE in equation (10) corresponding to the parameter values used in the previous plot for the ODEs The top two plots are evidence that not all parameter combinations yield localized solutions to the PDE, while some do, as seen in the bottom two plots. In the top two plots the PDE is initialized by a centered Gaussian pulse that splits into two waves that travel quickly throughout the medium and interacting with the boundary. In the bottom two plots however, the initial pulse remains localized in space, either dying out or traveling with positive amplitude. Although additional numerical simulations are needed, there is repeated evidence that the parameter γ is probably responsible for slip localization in these solutions. The plot on the bottom right suggests that under these parameter values, the friction law alone can be a mechanism to halt rupture propagation.

the emergence of these types of solutions may be directly affected by the parameters λ and μ, (the spring constant connecting each block to the driver plate, and the spring constant between blocks in the original, discrete formulation). This coincides with the findings of Español [1994] who found the localization dependent on the speed of sound $l^2 = \frac{\mu}{\lambda}$. In the case of the localized (breather) solutions, in some parameter regimes the amplitude of this localized pulse decays over time, as viewed in the bottom right plots in Figures 14 and 15.

Figure 14 shows four different numerical solutions to the ODEs (8) where a chain of 20 blocks is considered. The parameters ϵ and ξ are fixed at values 1 and 1.84, respectively, while γ and $\tilde{\gamma}$ are allowed to vary. In the top left plot in Figure 14, we see that for this set of parameter values, the initial Gaussian pulse splits into two solitary waves that travel through the medium and interact with the boundary. In the top right plot of this same Figure however, the initial pulse does not propagate like a traveling wave, suggesting that not all parameter combinations yield localized or solitary wave like solutions. The bottom two figures show solutions where the slip does not propagate throughout the medium, but remains localized or quasi-localized in the center of space, suggesting the presence of breather solutions. In these cases the slip either dies out (as in the bottom right of Figure 14), or maintains its amplitude and "breathes" (seen in the left of the same Figure). These solutions suggest that both γ and $\tilde{\gamma}$ may be responsible for this localization, but the value of γ probably affects whether or not the slip amplitude dies out, as $\tilde{\gamma}$ takes the same value in the bottom two plots.

We are interested if solitary or localized solutions occur for the PDE in equation (10) under similar conditions to the ODEs (8), or if the qualitative behavior changes in the continuum case. Figure 15 shows solutions to the PDE with the same parameter values and one can see, when comparing these plots to those in Figure 14, that for these sets of parameter values the dynamics are fairly similar, although we cannot compare them absolutely as the PDE is determined by the additional parameter c.

To investigate the behavior when two of these solitary waves meet, we take a solution that resembles a soliton and initialize it with two smooth Gaussian pulses, with different amplitudes. Figure 16 shows the profiles at different times for the interaction of these two pulses. The two initial pulses each split into two waves of the same form, then meet, and maintain the same form after the interaction. This is further evidence that our numerical solutions are solitons.

It is important to note, however, that the PDE in equation (10) can be re-scaled so that it is independent of the wave speed c. More specifically, we can scale the spatial variable x by c, replacing x by cx and yielding the following, re-scaled PDE:

$$\left. \begin{array}{l} u_{tt} = u_{xx} - \tilde{\gamma}^2 u - (\gamma^2/\xi)(\theta + \ln(u_t + 1))) \\ \theta_t = -(u_t + 1)(\theta + (1 + \epsilon)\ln(u_t + 1)) \end{array} \right\} \tag{12}$$
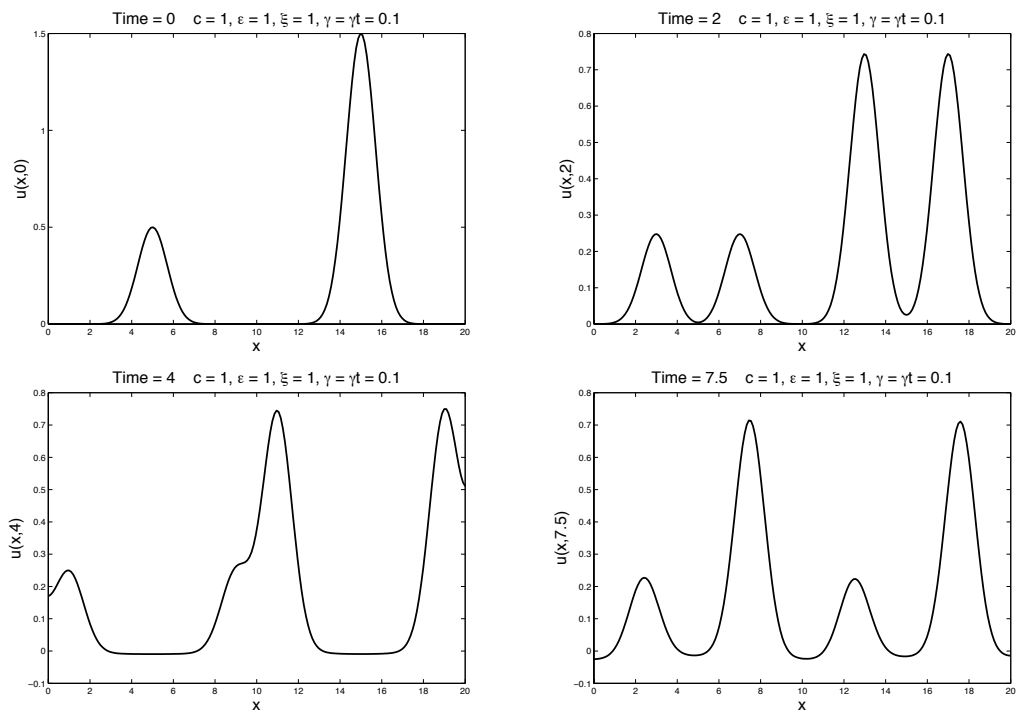
30

Figure 16: Soliton solutions at varying times. Initialized with 2 smooth Gaussian pulses, each wave splits into two waves that maintain the same shape after they pass through each other.
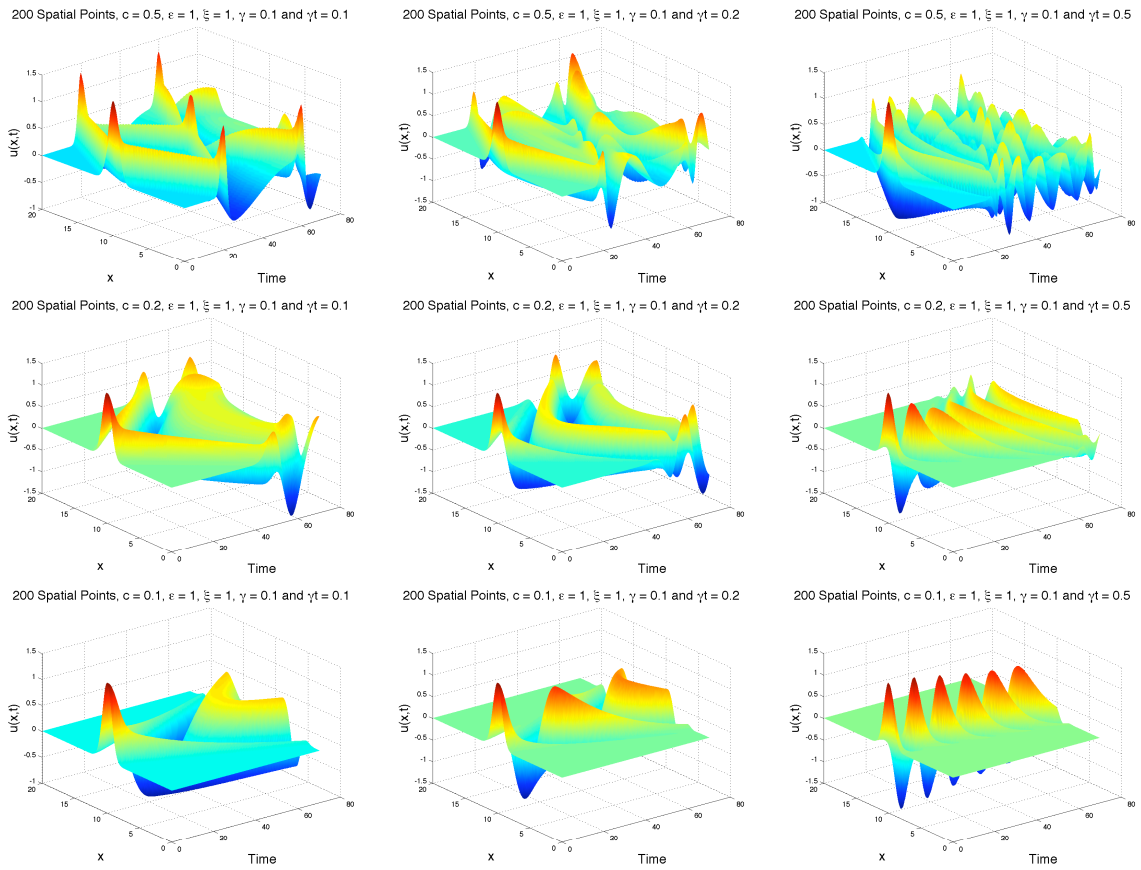
Figure 17: 0 plots showing the localization of slip as a function of the parameter $\tilde{\gamma}$. Moving from left to right corresponds to increasing the value of $\tilde{\gamma}$. Increasing $\tilde{\gamma}$ will cause the solution to localize as well as cause the slip to decrease in amplitude.

In this framework, we can ignore the effect of varying the wave speed, and instead view the equations of motion in terms of the driving term $\tilde{\gamma}^2$, i.e., the term corresponding to the pull of the driver plate (and the parameter responsible for loading energy into the system) and the damping term $\frac{\gamma^2}{\xi}$, the parameter controlling the amount of friction acting on the system. With these parameters in mind, we can control the behavior of the system by means of a single perturbation parameter,

$$\zeta = \frac{\text{drive}}{\text{damping}} = \frac{\tilde{\gamma}^2}{\gamma^2/\xi} = \frac{\tilde{\gamma}^2\xi}{\gamma^2},$$

the ratio of the drive to the damping.

We are interested in determining the role that ζ plays in the emergence of these traveling waves or localized solutions. Figure 17 shows results from the solutions to the PDE in equation (10) in a parameter-varying study. Since increasing the control parameter ζ is analogous to keeping ξ and γ fixed while increasing $\tilde{\gamma}$, these figures demonstrate the effect that the control parameter has on the system. Figure 17 shows a set of 9 plots of solutions to the PDE when the control parameter $\zeta = \frac{\tilde{\gamma}^2\xi}{\gamma^2}$ is increased (from top to bottom). One can also observe that the plots in the left 2 columns illustrate how the initial Gaussian pulse splits into two waves that travel outwards through the boundary. But in moving from top to bottom, the slip pulse is squeezed together so that it takes longer to interact with the boundary. This is evidence that an increase in the control parameter will cause the slip to localize, as well as die out in some cases. This makes sense as one can consider increasing ζ as analogous to increasing $\tilde{\gamma}$ (effectively increasing the pull of the driver plate so that it forces the chain of blocks to slide at steady state). One can further view this effect as analagous to crossing under the Hopf bifurcation plane seen in Figure 18, where parameter combinations yield stationary solutions.

4.4   Analytical Investigation of Soliton Solutions

In this section we investigate whether we can analytically determine the parameter spaces for which these solitary wave solutions occur. The original PDE (written with wave speed c_o) is:

$$\left.\begin{array}{l} u_{tt} = c_o^2 u_{xx} - \tilde{\gamma}^2 u - (\gamma^2/\xi)(\theta + \ln(u_t + 1))) \\ \theta_t = -(u_t + 1)(\theta + (1 + \epsilon)\ln(u_t + 1)) \end{array}\right\} \tag{13}$$

We now consider a solution to (13) of the form $h(x + ct)$, i.e. a traveling wave solution with wave speed c. Letting $\psi = x + ct$, and plugging h into the PDE yields the following ODE:
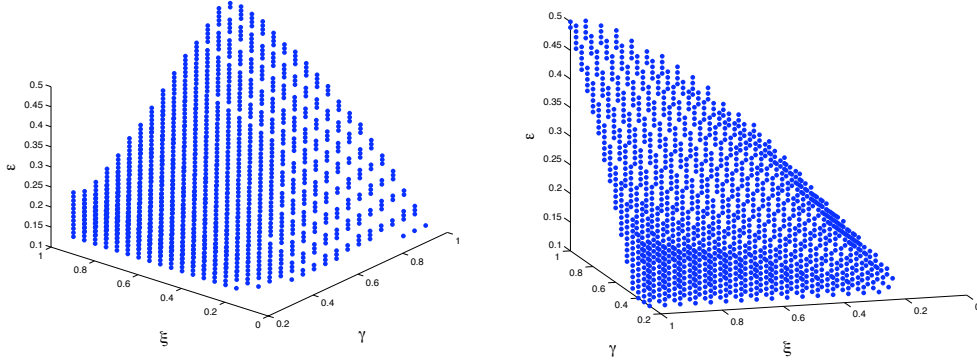
33

Figure 18: 2 different views of the bifurcation surface associated with equation (15), where $\gamma = \tilde{\gamma}$. Parameter combinations that lie below the surface will generate stationary solutions, while a combination above the surface will correspond to a Hopf bifurcation, and yield a periodic orbit. That it is a skewed surface for the parameter space we consider implies that the Hopf bifurcation is dependent on all three parameters ϵ, ξ and γ.

$$\left.\begin{array}{l}(c^2 - c_o^2)\frac{d^2 h}{d\psi^2} = -\tilde{\gamma}^2 h - (\gamma^2/\xi)(\theta + \ln(c\frac{dh}{d\psi} + 1))) \\ c\frac{d\theta}{d\psi} = -((c\frac{dh}{d\psi} + 1)(\theta + (1 + \epsilon)\ln(c\frac{dh}{d\psi} + 1))\end{array}\right\} \tag{14}$$

This second order ODE can be re-written as a system of first order ODEs by letting $u = h$ and $v = \frac{dh}{d\psi}$.

$$\left.\begin{array}{l}\frac{du}{d\psi} = v \\ (c^2 - c_o^2)\frac{dv}{d\psi} = -\tilde{\gamma}^2 u - (\gamma^2/\xi)(\theta + \ln(cv + 1))) \\ \frac{d\theta}{d\psi} = -\frac{1}{c}((cv + 1)(\theta + (1 + \epsilon)\ln(cv + 1))\end{array}\right\} \tag{15}$$

To do stability analysis of the ODE (15), we look first for the stationary solution, and find it at $(u, v, \theta) = (0, 0, 0)$. Then we look at the Jacobian matrix of equation (15):

$$Df = \begin{bmatrix} 0 & 1 & 0 \\ \frac{-\tilde{\gamma}^2}{c^2 - c_0^2} & \frac{-\gamma^2 c}{\xi(c^2 - c_0^2)(cv + 1)} & \frac{-\gamma^2}{\xi(c^2 - c_0^2)} \\ 0 & -(1 + \epsilon)(\ln(cv + 1) + 1) & -\frac{cv + 1}{c} \end{bmatrix}$$

and Df evaluated at the stationary solutions yields:

$$A = \begin{bmatrix} 0 & 1 & 0 \\ \frac{-\tilde{\gamma}^2}{c^2 - c_0^2} & \frac{-\gamma^2 c}{\xi(c^2 - c_0^2)} & \frac{-\gamma^2}{\xi(c^2 - c_0^2)} \\ 0 & -(1 + \epsilon) & -\frac{1}{c} \end{bmatrix}$$

34

It is important to note that, other than the presence of the parameters c and c_0 (which can be eliminated by scaling the equations appropriately in space, see equation (12)), matrix A is almost an exact copy of that obtained in Erickson et al. [2008], for the equations governing a single block. Just as before, matrix A has 3 distinct eigenvalues: 1 real eigenvalue and 2 complex conjugates. When the real part of the complex conjugates crosses the imaginary axis, the system in equation (15) undergoes a Hopf bifurcation from a stationary solution into a periodic orbit (see [Guckenheimer and Holmes, 1983] and [Perko, 2001]), as occurred in the single-block case in Erickson et al. [2008].

Figure 18 shows the parameter combinations that will yield bifurcations of the stationary state. Not surprisingly, it appears similar to the surface computed in Erickson et al. [2008] for the single block case, thus a similar analysis of the bifurcation plane can be made. Parameter combinations that lie below this plane will generate stationary solutions to equation (15), but once the parameter values have crossed this Hopf bifurcation plane, we see either periodic solitary wave type solutions or periodic localized solutions like those in the first 3 plots in Figures 14 and 15. We can use the information obtained from the study of the single block (see Erickson et al. [2008]) to predict that a similar route to chaos exists for the ODE (15) derived from considering soliton solutions to the PDE (10). In this case, increasing the value of the paramter ϵ will correspond to a period doubling cascade into chaos, resulting in solitary wave solutions that are aperiodic in time, although ϵ will need to be on the order of ≈ 11, as before. The assertion of this result would suggest that solitary wave-type solutions in the continuum formulation undergo behavioral changes on the same order of parameter values as in the single block case.

5   Discussion: Implications on the Scaling of the Friction Law

It has been widely recognized that our understanding of the physical mechanisms controlling earthquake rupture depends significantly on understanding the role of friction (see [Brace and Byerlee, 1966], [Scholz, 1998], among others). We believe that earthquakes and the resulting ground motions are affected by at least four factors, including initial stress, fault geometry, fault frictional behavior, and wave-propagation path effects. Of these, geometry and wave-propagation are somewhat possible to predetermine, the spatial distribution of the initial stress can be modeled according to the stochastic model discussed in Lavallée et al. [2006] (for applications see Schmedes et al. [2010a] and Schmedes et al. [2010b]) , but fault friction is still a major unknown. This makes understanding fault friction a cornerstone of understanding earthquake behavior. As highlighted in Harris [2004], earthquakes are the result of processes in the earth's crust that have evolved over multiple scales in both time and space. Understand-

ing the physics of earthquakes requires the study of these processes at all scales from both an observational and a dynamic modeling perspective.

That the transition to chaos for the discrete and continuum model with D-R friction ensues for a smaller parameter value than in the case of a single block may be an indication that a careful rescaling of the friction law is necessary, prior to attaching the friction law to full scale models. A similar conclusion was made by Schmittbuhl et al. [1996] who studied a "hierarchical array of blocks" and found that velocity weakening friction was scale dependent. These authors studied the bulk response of a two-dimensional elastic body sheared over a rough surface defined by a the velocity weakening friction law. They found that this friction law can produce Coulomb-like behavior at the system scale. More specifically, the velocity dependence of the body at the interface is lost or blurred when moving to larger scales. They conclude by emphasizing the need to study scale dependent effects of friction laws with an intrinsic length scale.

Our results suggest that when implementing the D-R friction law in dynamic rupture models, it's possible that qualitative behavior can be lost or altered when considering full-scale models. However it is possible to investigate the evolution of the scaling properties of numerical solutions to equations involving the friction law. Unfortunately, the presence of nonlinear terms in the mathematical formulation of friction laws like the D-R law makes it very difficult to define a transformation from laboratory scales to full scale models of the earth's faults. Another hypothesis will consist of formulating an "effective friction law" for length scales on the order of 100 m, much like the pioneering work of Campillo et al. [2001] who explored how small-scale variability in the parameters of the friction law can be renormalized to larger length scales.

6   Conclusions

We have derived the equations for both the discrete and the continuous formulations of a one-dimensional Burridge and Knopoff [1967] spring-block model subject to the nonlinear Dieterich-Ruina friction law. In the discrete case we observe a transition to chaos when varying the system size, i.e. the number of blocks N. For $N = 3$, 10, and 20 blocks, periodic behavior emerges. When N is increased from 20 to 21 however, this periodic behavior is lost and chaos ensues, as further asserted by the broadband noise in the power spectrum (see Figure 7). This transition occurs for a fixed set of parameter values and we see that the small value of $\epsilon = 0.5$ will generate chaotic motion, as long as the system size N is sufficiently large. This value is much smaller than that required for chaotic motion that we found in the single block case [Erickson et al., 2008], where $\epsilon \approx 11$. This suggests that, in contrast to the conclusions made by Lapusta and Rice [2003] who found only periodic behavior emerging from D-R friction, dynamic rupture modeling with this friction law can produce chaotic dynamics when considering

a wide range of parameter values with an increase in system size. It is possible that the parameter values selected by the authors, or their regularization of the D-R friction law prohibited the emergence of chaotic dynamics.

Also, these results suggest that chaotic regimes in the BK model under D-R friction is a function of the number of blocks considered, similar to the conclusions of Schmittbuhl et al. [1993] who studied a similar block-spring model subject to a velocity weakening friction law and found that chaos was also dependent on the system size. It should be emphasized that this information reveals that the D-R friction law may very well be scale-dependent, as we have seen different dynamics emerge in systems with different numbers of blocks. That the transition to chaos appears highly sensitive to the number of blocks N as well as the value of the parameter ϵ suggests that one should take into consideration their system size when choosing the parameters for a dynamic rupture model, or find another means of scaling the friction law appropriately. Because aperiodic solutions appear for smaller values of this specific parameter than in the case for a single block, it's probable that chaotic dynamics emerge for a broader range of parameter values for systems of larger size. Our numerical solutions so far suggest that the critical value of the parameter ϵ necessary to induce chaos decreases as a function of N, the numbers of blocks considered (for a hypothetical curve, see Figure 25 in Erickson [2010]).

For the continuum model of blocks and springs subject to the nonlinear D-R friction law, a bifurcation from a stationary state (steady sliding) to chaotic behavior can be observed when the parameter ϵ is increased, as further asserted in the power spectrum (see Figure 12). Recall that ϵ is the ratio of the stress parameters $(B - A)$ and A in the D-R friction law. Our results in this section show that $\epsilon = 1$ is sufficient for chaos in the PDE, a much smaller value than that required for chaotic motion in the single block system in Erickson et al. [2008], where $\epsilon \approx$ 11. It is important to note that we found chaotic behavior in the continuum model for different combinations of parameter values at even smaller values, namely for $\epsilon = 0.5$, however a clear transition from stationary to periodic to chaotic was not evident.

Although it is difficult to compare absolutely the discrete and the continuum model due to the second model's fourth parameter c, in either case the critical value for ϵ is much smaller than in the case of a single block, where $\epsilon \approx 11$. Our results suggest that for a fixed set of parameters, the critical value for ϵ decreases with N, the number of blocks considered. In the future it will be interesting to find the relationship between N and the critical value for ϵ, while keeping the other parameters fixed. In particular, it will be important to establish if this relationship depends on the values taken by the other parameters. Given the scale size of the model, the corresponding value taken by ϵ could be a useful method for controlling the observation of periodic or chaotic earthquake ruptures.

Furthermore, when we consider that $\epsilon = 1/S$, where S is the nondimensional seismic ratio [Andrews, 1976], smaller values of ϵ that yield chaotic dynamics correspond to a broader range

37

of S values. We found that in the single-block case, critical values of ϵ were large, corresponding to $S \approx \frac{1}{10}$ or smaller. Although we concluded in Erickson et al. [2008] that earthquake ruptures generated by chaotic simulations from a single block model correspond to velocities propagating at the supershear speed (see among others, [Freund, 1979], [Dunham, 2007]), for these models with more than one block chaotic regimes can be reached for a larger range of S values. In these cases, we find chaotic regimes corresponding to $S = 2$ or smaller.

In addition to these transitions from periodic to chaotic behavior, we have also observed that both the discrete and the continuous formulation of the Burridge-Knopoff block and spring model subject to the D-R friction law exhibit solutions where an initial, smooth Gaussian pulse can either split into two traveling waves that propagate as solitons, or remain localized in space, as breathers. In spite of having only explored a small region of the parameter space, we were able to determine which internal parameters seem to affect this behavior. Because these solitonic or localized solutions can be understood as a proxy for the propagation of the rupture across the fault during an earthquake ([Heaton, 1990]), this result may also suggest a possible range for parameters that could be used in future earthquake modeling. By narrowing the parameter space to values that yield localized solutions, we may have a method for assigning appropriate values to parameters that have, thus far, been difficult to determine.

Furthermore, a robust friction law is vital for dynamic rupture modeling of earthquakes, but evokes the question of whether or not small-scale laboratory derived friction laws are appropriate for full-scale modeling and modeling at high slip speeds. We have shown that finding pulse-like solutions in the continuum model reduces to studying the bifurcation analysis of a single block. Thus it is possible that using parameters relevant to the single block case under D-R friction may be directly applicable to large-scale models if one is interested in generating pulse-like solutions. This knowledge could be an indirect way for validating the use of a small-scale, laboratory derived friction law in full-scale dynamic rupture models.

An additional observation we made in this study is that for certain parameter combinations, the initial slip pulse in the BK model with D-R friction tends to die over time (as in the plots in the bottom right of Figures 14 and 15). Now the earthquake rupture process can be roughly divided into three parts: nucleation, propagation and arrest. But although rupture can be initiated in dynamic models of earthquakes by stress perturbations in initial conditions, an appropriate technique for terminating rupture is still unclear. Many dynamic models of earthquakes impose an artificial mechanism for stopping the rupture. The stopping criterion invoked by Ma et al. [2008] for example, solves for a traction value that will force the slip rate to die at the next time step during the dynamic rupture. The dying pulse in the bottom right plot of Figures 14 and 15 suggest that the friction law alone can provide a sufficient mechanism for halting the rupture process. In these cases where the slip amplitude decays, the dying pulse suggests that a localized rupture can propagate along the fault and be attenuated over a finite fault length. The

plots in the bottom right of Figures 14 and 15 suggest that properly choosing parameters of the friction law will be sufficient in halting rupture propagation. Having determined the parameter responsible for causing the slip to decay naturally, this parameter can be made a function of time and/or space in order to have a method for dynamically terminating slip events.

Under the Dieterich-Ruina law we may have discovered only a small subset of solutions to both the discrete and the continuous model, but there is no question that even in one spatial dimension, a rich phenomenology of dynamics exists. Furthermore, the presence of chaotic regimes and localized solutions are of great importance because they help justify the use of a relatively simple model in studies of fault friction, whereas more sophisticated dynamic models may be computationally limited.

7   Acknowledgments

Bibliography

J.-P. Ampuero and A. M. Rubin. Earthquake nucleation on rate and state faults - aging and slip laws. *J. Geophy. Res.*, 113:1–21, 2007.

D. J. Andrews. Rupture velocity of plane strain shear cracks. *J. Geophy. Res.*, 81:5679–5687, 1976.

U. M. Ascher and L. R. Petzold. *Computer methods for ordinary differential equations and differential- algebraic equations.* SIAM, first edition, 1998.

B. Birnir. Qualitative analysis of radiating breathers. *Comm. Pure Appl. Math.*, 47:103–119, 1994.

B. Birnir, H. McKean, and A. Weinstein. The rigidity of sine-gordon breathers. *Comm. Pure Appl. Math.*, 47:1043–1051, 1994.

W. F. Brace and J. D. Byerlee. Stick-slip as a mechanism for earthquakes. *Science.*, 153: 990–992, 1966.

R. Burridge and L. Knopoff. Model and theoretical seismicity. *Bull. Seism. Soc. Am.*, 57: 341–371, 1967.

M. Campillo, P. Favreau, I. R. Ionescu, and C. Voisin. On the effective friction law of a heterogeneous fault. *J. Geophy. Res.*, 106:16307–16322, 2001.

J. M. Carlson and J.S. Langer. Mechanical model of an earthquake fault. *Phys. Rev. A*, 40: 6470–6484, 1989.

J. M. Carlson, J. S. Langer, B. E. Shaw, and C. Tang. Intrinsic properties of a burridge-knopoff model of an earthquake fault. *Phys. Rev. A*, 44(2):884–897, 1991.

S. M. Corish, C. R. Bradley, and K. B. Olsen. Assessment of a nonlinear dynamic rupture inversion technique applied to a synthetic earthquake. *Bull. Seism. Soc. Am.*, 97:901–914, 2007. doi: 10.1785/0120060066.

E. G. Daub and J. M. Carlson. A constitutive model for fault gouge deformation in dynamic rupture simulations. *J. Geophy. Res.*, 113(B12309):1–20, 2008. doi: 10.1029/2007JB005377.

J. Dieterich. Time-dependent friction and the mechanics of stick-slip. *Pure appl. Geophys.*, 116:790–806, 1978.

J. H. Dieterich and B. D Kilgore. Direct observation of frictional contacts: new insights for state dependent properties. *Pure Appl. Geophys.*, 143:283–302, 1994.

E. M. Dunham. Conditions governing the occurrence of supershear rupture under slip weakening friction. *J. Geophy. Res.*, 112(B07302), 2007. doi: 10.1029/2006JB004717.

A. E. Elbanna and T. Heaton. Statistics of a dynamical system failing at multiple length scales and its implications on material strength, 2009. Poster presented at the Southern California Earthquake Center (SCEC) annual meeting, Palm Springs, Calif. 12-16 September 2009, abstract published in Proceedings and Abstracts, Volume XIX.

B. Erickson. *Complexity in the nonlinear Dieterich-Ruina friction law*. PhD dissertation, University of California, Santa Barbara, Department of Mathematics, June 2010.

B. Erickson, B. Birnir, and D. Lavallée. A model for aperiodicity in earthquakes. *Nonlin. Processes Geophys.*, 15:1–12, 2008.

P. Español. Propagative slipping modes in a spring-block model. *Phys. Rev. E*, 50:227–235, 1994.

L. B. Freund. The mechanics of dynamic shear crack propagation. *J. Geophys. Res.*, 84(B5): 2199–2209, 1979.

U. Frisch. *Turbulence: the legacy of A.N. Kolmogorov*. Cambridge University Press, 1st edition, 1995.

J. Guckenheimer and P. Holmes. *Nonlinear oscillations, dynamical systems, and bifurcations of vector fields*. Springer-Verlag, first edition, 1983.

R. Harris. Numerical simulations of large earthquakes: dynamic rupture propagation on heterogeneous faults. *Pure appl. geophys.*, 161:2171–2181, 2004.

T. H. Heaton. Evidence for and implications of self-healing pulses of slip in earthquake rupture. *Phys. Earth. Planet. Inter.*, 64:1–20, 1990.

S. Kichenassamy. Breathers and the sine-gordon equation. *Am. Math. Soc.*, 122:73–76, 1991.

L. Lapusta and J. Rice. Nucleation and early seismic propagation fo small and large events in a crustal earthquake model. *J. Geophy. Res.*, 108:1–18, 2003.

D. Lavallée, P. Liu, and R. J. Archuleta. Stochastic model of heterogeneity in earthquake slip spatial distributions. *Geophys. J. Int.,*, 165:622–640, 2006.

S. Ma, S. Custódio, R. J. Archuleta, and P. Liu. Dynamic modeling of the 2004 m_w 6.0 parkfield, california, earthquake. *J. Geophy. Res.*, 113:1–16, 2008.

R. Madariaga. Study of an oscillator of single degree of freedom with dieterich-ruina rate and state friction. *Unpublished Notes (Preprint)*, 1998.

R. Madariaga and K. B. Olsen. Earthquake dynamics. *International handbook of earthquake and engineering seismology*, 81A, 2002.

C. Marone. Laboratory-derived friction laws and their application to seismic faulting. *Annu. Rev. Earth Planet. Sci.*, 26:643–696, 1998.

R. E. Mickens. *Mathematical methods for natural and engineering sciences*. World Scientific Publishing Co. Pte. Lted., first edition, 2004.

H. Noda, E. M. Dunham, and J. R. Rice. Earthquake ruptures with thermal weakening and the operations of major faults at low overall stress levels. *J. Geophy. Res.*, 114(B07302), 2008. doi: 10.1029/2008JB006143.

M. Ohnaka and L-F. Shen. Scaling of the shear rupture process from nucleation to dynamic propogation: implications of geometric irregularity of the rupturing surfaces. *J. Geophy. Res.*, 104:817–844, 1999.

H. J. Pain. *The physics of vibrations and waves*. John Wiley & Sons, Ltd., Great Britain, second edition, 1968.

L Perko. *Differential equations and dynamical systems*. Springer-Verlag, New York, third edition, 2001.

S. Peyrat, K. Olsen, and R. Madariaga. Which dynamic rupture parameters can be estimated from strong ground motion and geodetic data? *Pure appl.geophys.*, 161:2155–2169, 2004.

E. Rabinowicz. The nature of the static and kinetic coefficients of friction. *J. Appl. Phys.*, 22: 1373–1379, 1951.

J. R. Rice. Heating and weakening of faults during earthquake slip. *J. Geophy. Res.*, 111 (B05311), 2006. doi: 10.1029/2005JB004006.

J. R. Rice. Constitutive relations for fault slip and earthquake instabilities. *Pure Appl. Geophys.*, 121:443–475, 1983.

J. R. Rice, N. Lapusta, and K. Ranjith. Rate and state dependent friction and the stability of sliding between elastically deformable solids. *J. Mech. Phys. Solids*, 49:1865–1898, 2001.

O. Rojas, E. M. Dunham, S. M Day, L.A. Dalguer, and J. E. Castillo. Finite difference modeling of rupture propagation with strong velocity-weakening friction. *Geophysical Journal International, submitted*, pages 1–21, 2009.

A. Ruina. Slip instability and state variable friction laws. *J. Geophy. Res.*, 88:10359–10370, 1983.

J. Schmedes, R. J. Archuleta, and D. Lavalleé. Correlation of earthquake source parameters inferred from dynamic rupture simulations. *J. Geophys. Res.*, 115, 2010a. doi: 10.1029/2009JB006689.

J. Schmedes, R. J. Archuleta, and D. Lavalleé. Dependency of supershear transition and ground motion on the autocorrelation of initial stress. *Tectonophysics, in press*, 2010b.

J. Schmittbuhl, Vilotte J.-P., and S. Roux. Propagative macrodislocation modes in an earthquake fault model. *Europhys. Lett.*, 21(3):375–380, 1993.

J. Schmittbuhl, J.-P. Vilotte, and S. Roux. Velocity weakening friction: a renormalization approach. *J. Geophy. Res.*, 101:13911–13917, 1996.

C. H. Scholz. *The mechanics of earthquakes and faulting*. Cambridge University Press, Cambridge, second edition, 2002.

C. H. Scholz. Earthquakes and friction laws. *Nature*, 391:37–42, 1998.

D. E. Sigeti. Exponential decay of power spectra at high frequency and positive lyapunov exponents. *Physica D*, 82:136–153, 1995.

D. Turcotte. *Chaos and fractals in geology and geophysics*. Cambridge University Press, second edition, 1997.

M. C. Valsakumar, S. V. M. Satyanarayana, and V. Sridhar. Signature of chaos in power spectrum. *Pramana J. of Physics*, 48(1):69–85, 1997.

W. Zhang, T. Iwata, K. Irikura, H. Sekiguchi, and M. Bouchon. Heterogeneous distribution of the dynamic source parameters of the 1999 chi-chi, taiwan, earthquake. *J. Geophy. Res.*, 108: 1–14, 2003.